UDC 621
CODEN: MINSC5
ISSN 1857 – 5293

MECHANICAL ENGINEERING SCIENTIFIC JOURNAL

МАШИНСКО ИНЖЕНЕРСТВО НАУЧНО СПИСАНИЕ

Volume 28
Number 1

Skopje, 2009

Mech. Eng. Sci. J.	Vol. **28**	No. 1	pp. 1–40	Skopje 2009
Маш. инж. науч. спис.	Год.	Број	стр.	Скопје

МАШИНСКО ИНЖЕНЕРСТВО – НАУЧНО СПИСАНИЕ
MECHANICAL ENGINEERING – SCIENTIFIC JOURNAL

Издава
Машински факултет, Универзитет „Св. Кирил и Методиј“, Скопје, Р. Македонија
Published by
Faculty of Mechanical Engineering, "SS. Cyril and Methodius" University, Skopje, R. Macedonia

Излегува два пати годишно – Published twice yearly

УДК: НУБ „Климент Охридски“ – Скопје (Оља Стојанова) — UDC: "St. Kliment Ohridski" Library – Skopje (Olja Stojanova)

Тираж: 300 — Copies: 300
Цена: 520 денари — Price: 520 denars

Адреса — Address
Машински факултет — **Faculty of Mechanical Engineering**
(Машинско инженерство – научно списание) — (Mechanical Engineering – Scientific Journal)
Одговорен уредник — Editor in Chief
пошт. фах 464 — P.O.Box 464
МК-1001 Скопје, Република Македонија — MK-1001 Skopje, Republic of Macedonia

Mech. Eng. Sci. J. is indexed/abstracted in INIS (International Nuclear Information System)
www.mf.ukim.edu.mk

МАШИНСКО ИНЖЕНЕРСТВО – НАУЧНО СПИСАНИЕ
МАШИНСКИ ФАКУЛТЕТ, СКОПЈЕ, РЕПУБЛИКА МАКЕДОНИЈА

MECHANICAL ENGINEERING – SCIENTIFIC JOURNAL
FACULTY OF MECHANICAL ENGINEERING, SKOPJE, REPUBLIC OF MACEDONIA

Mech. Eng. Sci. J.	Vol.	No.	pp.	Skopje
	28	1	1–40	2009
Маш. инж. науч. спис.	Год.	Број	стр.	Скопје

С О Д Р Ж И Н А

MECHANICAL ENGINEERING – SCIENTIFIC JOURNAL
FACULTY OF MECHANICAL EGINEERING, SKOPJE, REPUBLIC OF MACEDONIA

МАШИНСКО ИНЖЕНЕРСТВО – НАУЧНО СПИСАНИЕ
МАШИНСКИ ФАКУЛТЕТ, СКОПЈЕ, РЕПУБЛИКА МАКЕДОНИЈА

Mech. Eng. Sci. J.	Vol.	No.	pp.	Skopje
	28	1	1–40	2009
Маш. инж. науч. спис.	Год.	Број	стр.	Скопје

C O N T E N T S

Mechanical Engineering – Scientific Journal, Vol. **28**, No. 1, pp. 1–5 (2009)
CODEN: MINSC5 – 400 ISSN 1857–5293
Received: October 16, 2008 UDK: 621.649.1
Accepted: April 7, 2009

Original scientific paper

NATURAL FREQUENCIES OF A BLADE GROUP WITH A LACING WIRE

Zlatko Petreski

Faculty of Mechanical Engineering, SS Cyril and Methodius University,
P.O Box 464, MK-1001 Skopje, Republic of Macedonia
zlatko@mf.edu.mk

A b s t r a c t: In this paper the results of the dynamic behavior (natural frequencies and mode shapes changes) for a group of two, three and five blades as a result of changes made with the lacing wire are presented. Generally, the influence of two changes of the lacing wire on the blade group natural frequencies: position on the blade and elasticity, will be analyzed. The investigation is made on the model of blade with rectangular cross section with or without stagger angle. First three tangential bending natural frequencies and mode shapes and influence of the lacing wire on them are discussed in this paper. Numerical calculation based on the finite element method and NISA package for determination of natural frequencies and mode shapes of packeted blades is used. Three-dimensional finite element models of the blade group are made by using twenty node isoparametric solid elements. The number of degrees of freedom is different for each model (more than 6000 DOF). The results of the investigation are given in tables and graphics of natural frequencies changes versus lacing wire position and natural frequencies changes versus lacing wire elasticity.

Key words: natural frequencies; lacing wire; blade group

1. INTRODUCTION

An accurate dynamic analysis of blades or blade groups is of a great interest for the reasonable design of the steam turbine. Operating practice of steam turbine shows that damages to blades constitute a considerable proportion of all the damages to the steam turbine, therefore the dynamic analysis of blades or blade groups is of great significance.

One of the most important dynamic parameters for any construction including turbomachine blades is its natural frequencies. One of the main steps for a good design of turbine blading is determination of natural frequencies and mode shapes. The natural frequency changes of turbine blade are directly connected with changes of the resonant stress response of blade.

A blade group exhibits more complex dynamic behavior than a free-standing blade. The cantilever mode frequencies are influenced by the nearest blades, the shroud and lacing wires mass and the elasticity. In addition to the cantilever modes, fixed-pinned modes appear in groups between the cantilever modes.

The work presented in this paper is a small part of a project that should contain an investigation connected with turbine blade fatigue behavior under static and dynamic stress fields especially in the zone of high stress, during the critical condition of blade operating, where the fatigue crack usually initiates.

This paper shows the results of investigation of the dynamic behavior (natural frequencies and mode shapes changes) for a group of two, three and five blades as a result of changes made with the lacing wire. Generally the influence of two changes of the lacing wire, its position on the blade and its elasticity will be analyzed. The investigation is made on the blade with the rectangular cross section with or without a stagger angle. First three tangential bending natural frequencies and mode shapes and influence of the lacing wire on them are discussed in this paper.

2. NUMERICAL INVESTIGATION

The numerical calculation of the natural frequencies is done by using a complex program package NISA which is based on the Finite Element Analysis Method. We choose this software because it contains a great number of modulus that help while generatings the mesh of the system model, and it gives opportunities of a detail structure analysis. These programs during the dynamic system analysis use the standard FEA model:

$$[\mathbf{K}]\,[\mathbf{D}] = [\mathbf{M}]\,[\mathbf{D}]\,[\mathbf{W}]^2$$

where [**K**] is stiffness matrix, [**M**] – mass matrix, [**D**] – displacement matrix (mode shapes), $[\mathbf{W}]^2$ –

diagonal matrix containing eigenvalues (natural frequencies).

For the purpose of the investigation more than thirty FE models described below were made:

- Group of two blades with a rectangular cross-section mounted on the root block without a stagger angle, connected with a lacing wire with a diameter of 3; 4; 5 and 6 mm, located at 0.5; 0.62; 0.75; 0.87 and 1.0 of the blade height (H) from the bottom (Fig. 1).
- Group of three blades with a rectangular cross-section mounted on the root block without a stagger angle, connected with a lacing wire with a diameter of 3; 4; 5 and 6 mm, located at 0.5; 0.62; 0.75; 0.87 and 1.0 of the blade height (H) from the bottom (Fig. 1).
- Group of five blades with a rectangular cross-section mounted on the root block without a stagger angle, connected with a lacing wire with a diameter of 3; 4; 5 and 6 mm, located at 0.5; 0.62; 0.75; 0.87 and 1.0 of the blade height (H) from the bottom (Fig. 1).
- Group of three blades with a rectangular cross-section mounted on the root block with a stagger angle of 20 and 40 degrees, connected with a lacing wire with a diameter of 3; 4; 5 and 6 mm, located at 0.5; 0.62; 0.75; 0.87 and 1.0 of the blade height (H) from the bottom.

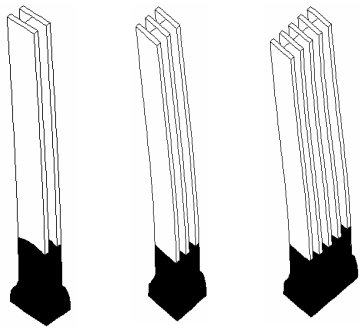

Fig. 1. FE models of group with two, three and five blades

The number of elements used to model each blade and blade group was different. Three dimensional twenty node isoparametric solid elements were used for blade modeling. The lacing wire was modeled with three dimensional beam elements.

3. RESULTS OF THE INVESTIGATION

A part of the results of the investigation in the graphics (Fig. 1 to Fig. 15) and Table 1 to Table 4 are given. The variation of the natural frequencies and mode shapes with the lacing wire elasticity and location changeing are shown.

On the Figs. 2, 4 and 6 the variation of the first, second and third tangential bending mode with the elasticity of the lacing wire for the blade group of two blades is shown.

On the Figs. 3, 5 and 7 the variation of the first, second and third tangential bending mode with the location of the lacing wire relative with the blade height for the blade group of two blades is shown.

On the Figs 8, 9 and 10 the variation of the first, second and third tangential bending mode with the location of the lacing wire relative with the blade height for the blade group of three blades is shown.

On the Figs. 11 and 12 the variation of the first, second and third tangential bending mode with the location of the lacing wire relative with the blade height for the blade group of five blades is showen.

Into the Table 1 to Table 3 the increase of the natural frequency of the first, second and third bending mode for the group of two, three and five balades are given.

The variation of the first three tangential bending modes and natural frequencies for the group of three blades connected with one lacing wire with d = 5 mm on the different location are given into the Table 4 and on the Fig. 13 to Fig. 15.

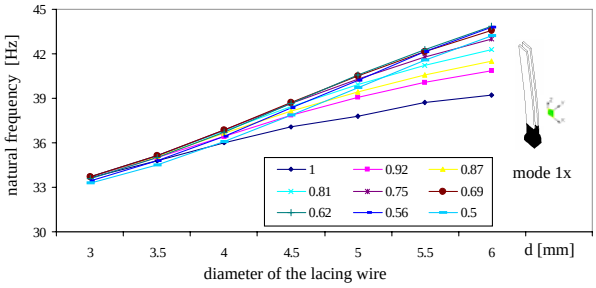

Fig. 2. Variation of the first bending mode with the elasticity of the lacing wire for the group of two blades

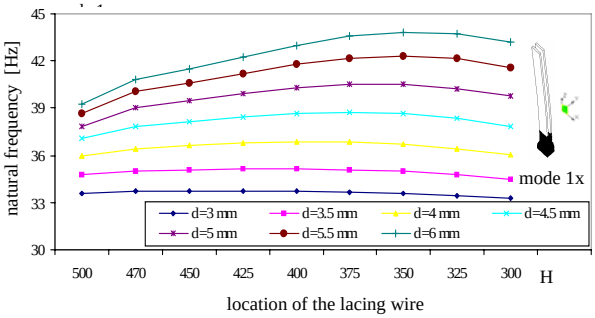

Fig. 3. Variation of the first bending mode with the height of the lacing wire for the group of two blades

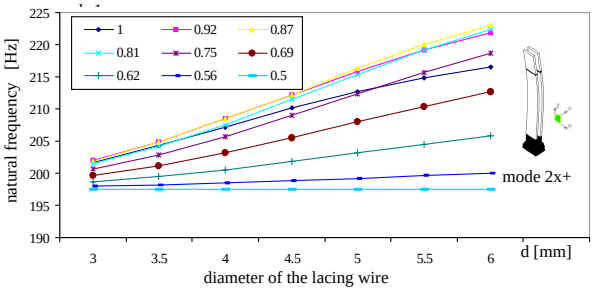

Fig. 4. Variation of the second bending mode with the elasticity of the lacing wire for the group of two blades

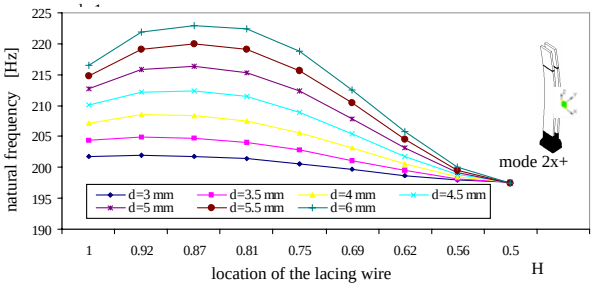

Fig. 5. Variation of the second bending mode with the height of the lacing wire for the group of two blades

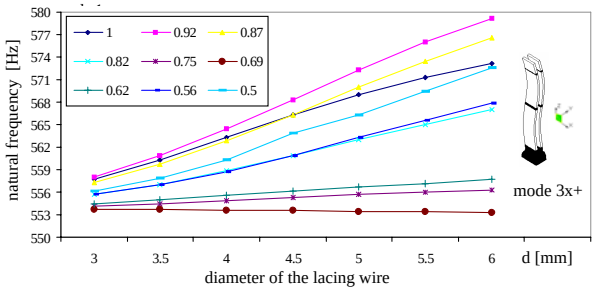

Fig. 6. Variation of the third bending mode with the elasticity of the lacing wire for the group of two blades

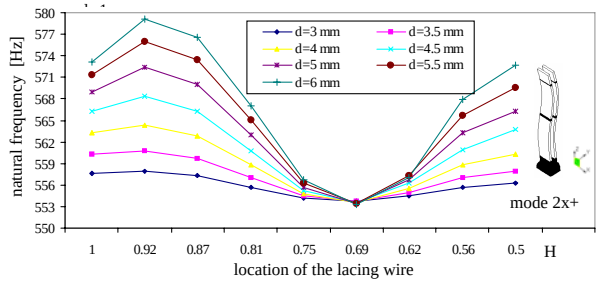

Fig. 7. Variation of the third bending mode with the height of the lacing wire for the group of two blades

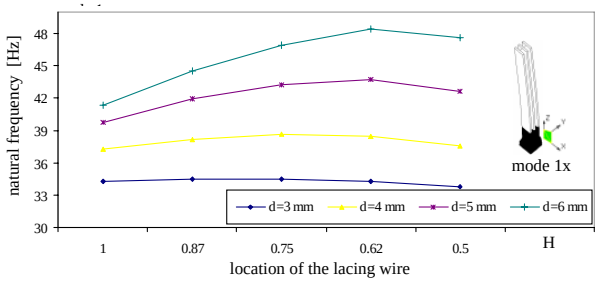

Fig. 8. Variation of the first bending mode with the height of the lacing wire for the group of three blades

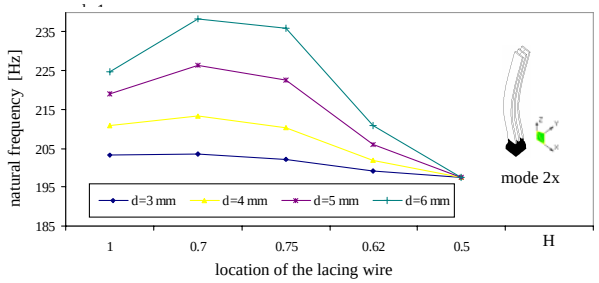

Fig. 9. Variation of the second bending mode with the height of the lacing wire for the group of three blades

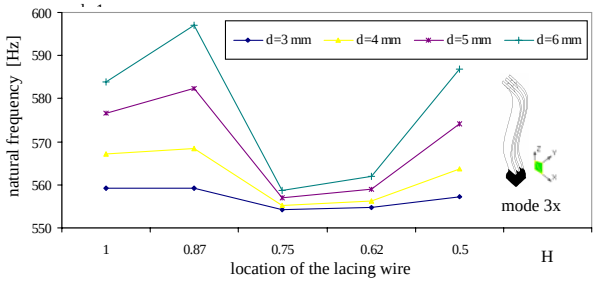

Fig. 10. Variation of the third bending mode with the height of the lacing wire for the group of three blades

Table 1

Increase of the natural frequency of the first bending mode (1×)

Nr. of blades in group	Stagger angle (°)	Location of the lacing wire (H)				
		1	0.87	0.75	0.62	0.5
		%	%	%	%	%
2	0	16.7	22.9	27.4	30.5	29.9
3	0	20.57	29.26	36.07	41.17	40.61
5	0	23.13	33.7	42.57	49.4	49.3
3	20	20.23	29.31	36.5	41.91	41.23
3	40	18.36	27.31	35.1	42.05	43.3

Table 2

Increase of the natural frequency of the second bending mode (2×)

Nr. of blades in group	Stagger angle (°)	Location of the lacing wire (H)				
		1	0.87	0.75	0.62	0.5
		%	%	%	%	%
2	0	7.3	10.47	9.00	3.57	0
3	0	10.62	17.1	16.72	5.94	0
5	0	13.01	22.29	23.45	8.05	0
3	20	11.13	18.18	17.84	6.85	0
3	40	10.74	18.68	19.82	7.96	1.09

Table 3

Increase of the natural frequency of the third bending mode (3×)

Nr. of blades in group	Stagger angle (°)	Location of the lacing wire (H)				
		1 %	0.87 %	0.75 %	0.62 %	0.5 %
2	0	2.77	3.45	0.5	0.7	2.96
3	0	4.42	6.78	0.8	1.3	5.28
5	0	–	–	–	–	–
3	20	4.49	7.01	0.8	1.38	5.54
3	40	4.6	7.7	0.97	2.36	6.6

Table 4

Variation of the first three tangential bending modes with the location of the lacing wire

	First three tangential bending modes		
	mode 1×	mode 2×	mode 3×
d = 5 mm			
1.0×H	39.78	219.03	576.57
0.92×H	41.32	224.85	583.54
0.87×H	41.92	226.44	582.3
0.81×H	42.64	226.8	569.96
0.78×H	43.28	226.58	562.38
0.75×H	43.24	222.66	556.87
0.69×H	43.64	213.98	553.28
0.62×H	43.73	206.08	558.9
0.56×H	43.42	200.3	568.31
0.5×H	42.66	197.51	574.23
0.44xH	41.46	197.86	567.9
0.37×H	39.91	200.62	558.75
0.31×H	38.15	204.27	553.13

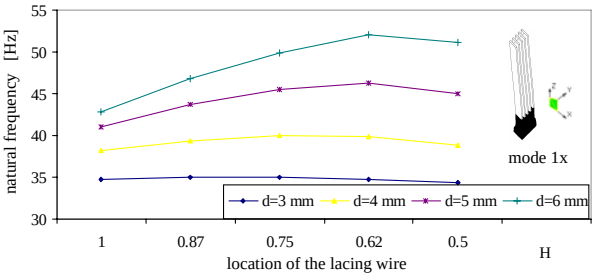

Fig. 11. Variation of the first bending mode with the height of the lacing wire for the group of five blades

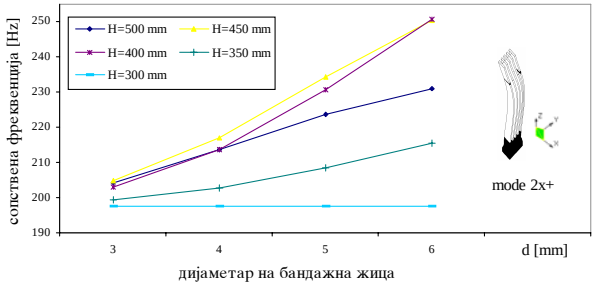

Fig. 12. Variation of the second bending mode with the height of the lacing wire for the group of five blades

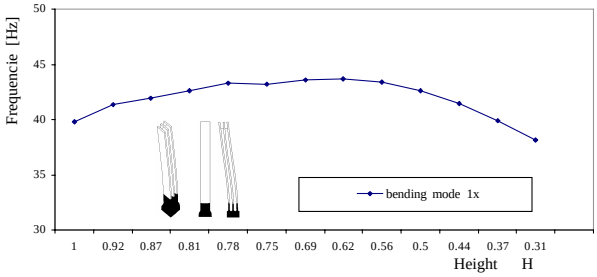

Fig. 13. Variation of the first bending mode with the height of the lacing wire

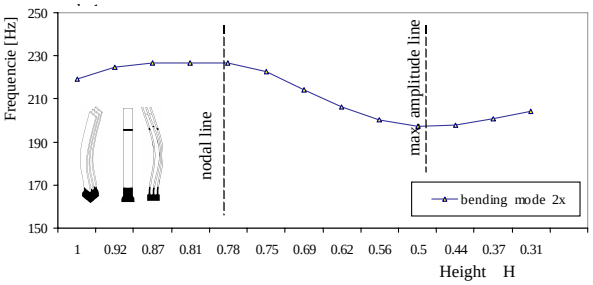

Fig. 14. Variation of the second bending mode with the height of the lacing wire

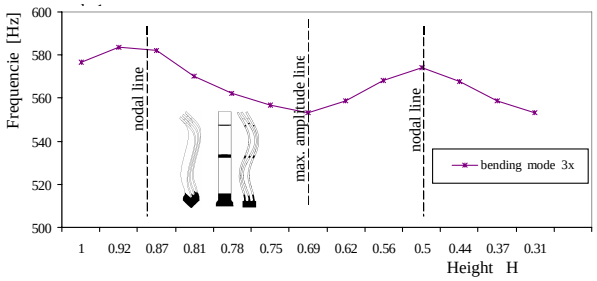

Fig. 15. Variation of the third bending mode with the height of the lacing wire

4. CONCLUSION

Based on the analysis of the numerical calculation the following conclusions about variation of the natural frequencies of the first three tangential bending modes for the groups of two, three and five blades can be made:

– All three blade groups (with two, three or five blades) show a very simular form of variation of the natural frequencies with the lacing wire elasticity or height location changes.

– The natural frequencies are increase with the increase of the diameter of the lacing wire (Figs. 2, 4 and 6).

– The natural frequencies are increase when the location of the lacing wire is near the nodal line of the mode, and decrease when the location of the lacing wire is near the line of the maximum amplitude of the mode (Figs. 14 and 15).

– When the location of the lacing wire is near the nodal line the natural frequencies change more with the diameter changes. On the other hand when the location of the lacing wire is near the line of the maximum amplitude of the mode the natural frequencies are not sensitive to the diameter changes (Tables 2 and 3).

– When the group is made of more blades (five) it becomes more sensitive to the elasticity of the lacing wire changes than the group with less blades (Table 1 to Table 3).

– The first bending mode and the natural frequency are more sensitive to the elasticity of the lacing wire changes, and the third mode has the smallest variations (Table 1 to Table 3).

– The increase of the stagger angle has small influence on the increase of all first three bending modes and natural frequencies (Table 1 to Table 3).

REFERENCIES

[1] J. S. Rao, *Turbomachine Blade Vibration*, New Delhi, Wiley Eastern Limited (1991).

[2] O. C. Zienkiewicz., *The Finite Element Method*, London, Mc Graw-Hill (1977).

[3] Z. Petreski, A. Ilievski, Some Aspects of the Natural Frequencies Changes Related with a Structural Discontinuity, *Proc. of 10-th World Congress on the Theory of Machines and Mechanisms*, Oulu, Finland, 1584–1588 (1999).

[4] USER'S MANUEL for NISA program.

Р е з и м е

СОПСТВЕНИ ФРЕКВЕНЦИИ НА ПАКЕТ ЛОПАТКИ СО БАНДАЖНА ЖИЦА

Zlatko Petreski

Машински факултет, Универзитет „Св. Кирил и Методиј“,
п. фах 464, МК-1001 Скопје, Република Македонија
zlatko@mf.edu.mk

Клучни зборови: сопствени фреквенции; бандажна жица; пакет лопатки

Во овој труд се прикажани резултатите од истражувањето на промените на динамичкото однесување (сопствени фреквенции и форми на тоновите) на пакети со две, три и пет лопатки, во зависност од бандажната жица. Во принцип, анализирано е влијанието на две карактеристики на бандажната жица врз сопствените фреквенции на пакетот: положбата на поставување на лопатката и крутоста. Истражувањата се направени на модели на лопатки со упростен, правоаголен напречен пресек, поставени под различен агол во однос на оската на роторот. Разгледувано е влијанието на бандажната жица врз сопствените фреквенции на првите три тона на свиткување во тангенцијален правец. За нумеричка пресметка и симулација на моделот користен е програмскиот пакет NISA, базиран на методот на конечни елементи. Моделите во пресметките се со различен број степени слобода на движење (повеќе од 6000 DOF). Добиените резултати се прикажани табеларно и во облик на дијаграми.

Mechanical Engineering – Scientific Journal, Vol. **28**, No. 1, pp. 7–12 (2009)
CODEN: MINSC5 – 401 ISSN 1857–5293
Received: December 8, 2008 UDK: 531.788.793
Accepted: January 14, 2009

Original scientific paper

MATLAB PROGRAM FOR CAM DESIGN OPTIMIZATION OF PLANAR CAM MECHANISMS WITH TRANSLATING ROLLER FOLLOWERS

Dame Korunoski, Ivan Mickoski, Hristijan Mickoski

Faculty of Mechanical Engineering, SS. Cyril and Methodius University,
P.O Box 464, MK-1001 Skopje, Republic of Macedonia
dame@mf.edu.mk / ivanm@mf.edu.mk / hristijanm@mf.edu.mk

A b s t r a c t: The problem of cam-profile determination and its optimization, as pertaining to cam mechanisms with translating roller followers, is analyzed in this paper. The key variables that need to be monitored for roller followers are the pressure angle and the cam-profile curvature. In this paper a Matlab program is made, based on "Symbolic Math Toolbox" that calculates a minimum radius of base circle (minimum cam size) under a maximum-pressure angle constraints and an optimum roller radius, so as to avoid the phenomenon known as undercutting, i.e. to avoid high contact stresses. The input program parameters are any function that describes a follower-displacement program, the maximum pressure angle, the rise of a follower and four phases such as lower dwell, rise phase, upper dwell, and return phase. So the output parameter is the optimum radius of the base circle, the optimum roller radius and the synthesized cam-profile. The program provides a visual graphical presentation of a synthesized cam-profile, its animation and calculates its geometric properties.

Key words: cam; roller; pressure angle; MATLAB

1. INTRODUCTION

The process of systematically choosing the mechanism parameters in order to produce a given displacement program of the follower, while minimizing the cam size and regarding all important constraints of mechanism variables, is called *cam design optimization*, that is a subject of analysis in this paper.

But, it is possible to choose values of the mechanism parameters to produce theoretically the prescribed motion of the follower which satisfies the underlying kinematic constraints, but it is structurally inadmissible or physically unfeasible. In fact, the profile synthesis procedure can generate curves that do not close, so that it is an unfeasible design, or curves that, although closed, contain cusps (a defect known as *undercutting*). The cusps are inadmissible because of the large contact stresses that they produce, and hence should be eliminated early in the design stage. In the case of translating roller followers, the conditions for cam size minimization and cusp elimination are discussed and analyzed below in this paper.

2. EMATICS RELATIONS FOR KNIFE-EDGE FOLLOWERS

The knife-edge translating follower, shown on Fig. 1, is not usually found in practice, because of large contact stresses that it produces. However, it has theoretical and practical importance for cam mechanisms with roller followers.

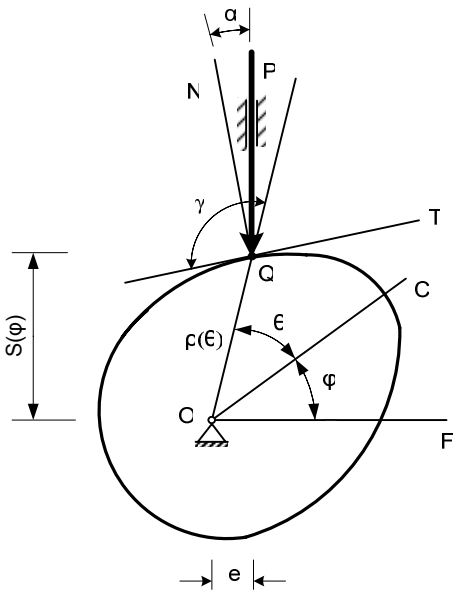

Fig. 1. Geometry of a cam with a translating knife-edge follower

Let us consider Fig.1, where OF and OC are lines attached to the fixed frame and to the cam respectively. Line P is the path of the tip of the fol-

lower, lines T and N are the tangent and the normal of the cam profile at the contact point Q. Moreover, φ and s denote an angular displacement of the cam and a translational displacement of the follower, where $\boldsymbol{s}$ can be considered as a sum of a constant $\boldsymbol{c}$, which is the *design variable*, as yet to be determined, plus a *positive-semidefinite* function $\sigma(\varphi)$ whose minimum value is zero and its maximum being equal to the total follower lift, h. Thus,

$$s(\varphi) = c + \sigma(\varphi) \tag{1a}$$

and hence,

$$s'(\varphi) = \sigma'(\varphi)\ , \qquad s''(\varphi) = \sigma''(\varphi)\,. \tag{1b}$$

Furthermore, let θ and $\rho(\theta)$ be the polar coordinates defining the contact point Q. From the geometry of Fig. 1, one can write

$$\begin{aligned} s(\varphi) &= \rho(\theta)\sin(\varphi+\theta)\ , \\ e &= \rho(\theta)\cos(\varphi+\theta) \end{aligned} \tag{2}$$

$$\alpha = \varphi + \theta + \gamma - \pi \tag{2a}$$

where α is the pressure angle, and γ can be obtained, regarding to the [1], by expression

$$\gamma = \tan^{-1}\left[\frac{\rho(\theta)}{\rho'(\theta)}\right]. \tag{2b}$$

From basic polar-coordinate relations, we have

$$x = \rho\cos\theta\ , \qquad y = \rho\sin\theta\ .$$

Upon expansion of eqs. (2), we obtain, respectively,

$$s = \rho\cos\theta\sin\varphi + \rho\sin\theta\cos\varphi$$

$$s = x\sin\varphi + y\cos\varphi \tag{3a}$$

$$e = \rho\cos\theta\cos\varphi - \rho\sin\theta\sin\varphi$$

$$e = x\cos\varphi - y\sin\varphi \tag{3b}$$

Next, eqs. (3a) and (3b) are rewritten in a vector form as

$$\begin{bmatrix}\cos\varphi & -\sin\varphi \\ \sin\varphi & \cos\varphi\end{bmatrix}\begin{bmatrix}x \\ y\end{bmatrix} = \begin{bmatrix}e \\ s\end{bmatrix} \tag{4}$$

or

$$\mathbf{Q}(\varphi)\mathbf{p}(\varphi) = \mathbf{r}(\varphi) \tag{5}$$

where matrix $Q(\varphi)$ being orthogonal, i.e.,

$$\mathbf{Q}^T\mathbf{Q} = \mathbf{Q}\mathbf{Q}^T = 1, \qquad \det(Q) = 1 \tag{6}$$

Furthermore, 1 denotes the 2×2 identity matrix, and hence eq. (5) can readily be solved for the the vector $\mathbf{p}(\varphi)$, namely,

$$\mathbf{p}(\varphi) = \mathbf{Q}^{\mathbf{T}}(\varphi)\,\mathbf{r}(\varphi) = \begin{bmatrix} s(\varphi)\sin\varphi + e\cos\varphi \\ s(\varphi)\cos\varphi - e\sin\varphi \end{bmatrix} \tag{7}$$

or

$$x = s(\varphi)\sin\varphi + e\cos\varphi \tag{8a}$$

$$y = s(\varphi)\cos\varphi - e\sin\varphi \tag{8b}$$

Note that $\mathbf{r}(\varphi)$ represents the coordinates of a point of the cam profile in a coordinate system fixed to the machine frame, and $\mathbf{p}(\varphi)$ represents those of the same point in a coordinate system fixed to the cam disk. Also note that eqs. (8a) and (8b) are needed for cam profile determination.

3. CAM PROFILE OPTIMIZATION UNDER A MAXIMUM PRESSURE-ANGLE CONSTRAINT

According to the [1], [2] the minimum radius of the base circle under a maximum pressure angle constraint is given as,

$$c = \frac{k_1}{2\tan\alpha_M} \tag{9a}$$

$$e = \frac{k_1}{2} \tag{9b}$$

$$b = \frac{k_1}{2\sin\alpha_M} \tag{9c}$$

where c is design variable, e is eccentricity (offset of the path of the follower tip), b is a minimum base radius and

$$k_1 = \sigma'(\varphi^*) - \tan\alpha_M\,\sigma(\varphi^*) \tag{9d}$$

where φ^* is a value that satisfying equation,

$$\sigma''(\varphi^*) - \tan\alpha_M\,\sigma'(\varphi^*) = 0\,,\ \ \varphi_a < \varphi < \varphi_b \tag{9e}$$

and $\Delta\varphi = \varphi_b - \varphi_a$ is the cam angle of rotation for the rise or the return phase.

4. CAM PROFILE DETERMINATION FOR THE ROLLER FOLLOWERS

In previous section, the Cartesian coordinates describing the cam profile for a translating knife-edge follower were obtained (8a) and (8b). Based on those results, the corresponding methodology

for determining the cam profile for a roller follower is explained bellow. The layout of this type of the cam mechanism is shown in Fig. 2.

Let $\mathbf{e_t}$, $\mathbf{e_n}$, and $\mathbf{r}$ be the unit tangent and normal vectors of the cam profile and its radius of curvature, respectively. If we are specifying a value a of the roller radius, the profile of the corresponding cam can be obtained from the relation,

$$\mathbf{r}_r = \mathbf{r}_k + a\ \mathbf{e}_n \tag{10}$$

where $\mathbf{r_r}$ and $\mathbf{r}_k$, shown in Fig. 3, are the position vectors of corresponding points – points sharing a common normal–on the cam profile for the roller and for the knife-edge followers, respectively.

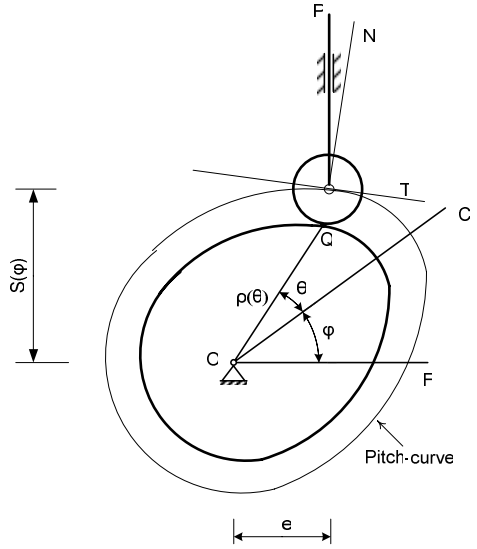

Fig. 2. Layout of a translating roller-follower cam mechanism

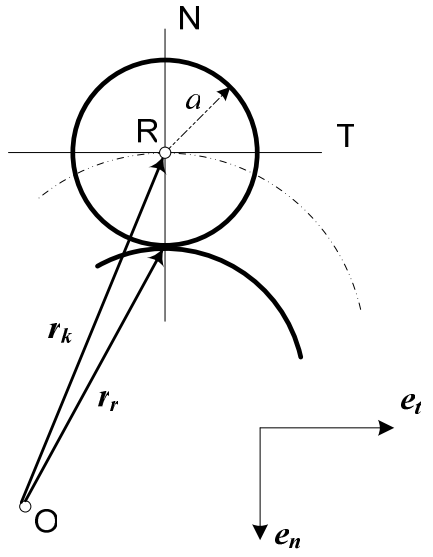

Fig. 3. Geometry of a cam profile and a path of the roller center R

According to the [1], the roller radius is given as a fraction ν of $\mathbf{r}_m$, the minimum absolute value of the radius of curvature, then

$$a = \nu\,\mathbf{r}_m = \frac{\nu}{k_M}, \qquad 0 < \nu < 1 \tag{11a}$$

where

$$k_M = \max_{\varphi}\left\{\left|k_k(\varphi)\right|\right\}, \quad 0 < \varphi < 2\pi \tag{11b}$$

$$k_k = \frac{s(s-s'') + (s'-e)(2s'-e)}{\sqrt{[s^2 + (s'-e)^2]^3}} \tag{11c}$$

and a values of φ are obtained as zeros of function $H(\varphi)$ given by the expression,

$$H(\varphi) = [s^2 + (s'-e)^2]\cdot[s(2s'-s''') + 3s''(s'-e)] -$$

$$-3[ss'+s''(s'-e)]\cdot[s(s-s'') + (s'-e)(2s'-e)]$$

So the design procedure is:

1. Determine the minimum base radius under a maximum pressure angle constraint (eq. 9c).

2. Find the zeros of the function $\mathbf{H}(\varphi)$. Using eqs. (11a), (8b) and (8c), calculate the roller radius.

3. Using eqs. (8a) and (8b), determine the cam profile for the corresponding cam without a roller (pitch-curve).

4. Based on the eq. (10), calculate the cartesians coordinates of the points of the cam profile with a roller.

5. CONCLUSION

Based on [1], [2], [3] and [4], we have made a MATLAB program that calculates the minimum radius of the base circle (minimum size cam) under a maximum-pressure angle constraint and an optimum roller radius for high contact stresses avoidance. The program also provides animation of the optimized and synthesized cam-profile and calculation of its geometric properties as well as centroid coordinates, cam area and principal moments of inertia. For one example it is presented in the appendix shown bellow.

APPENDIX

1. Figure 4: MATLAB program for cam design optimization and determination of its geometric properties.

2. Figure 5: Determination of the cam profile.

3. Figure 6: Determination of the geometric properties of cam.

4. Figure 7: Principal axes of inertia.

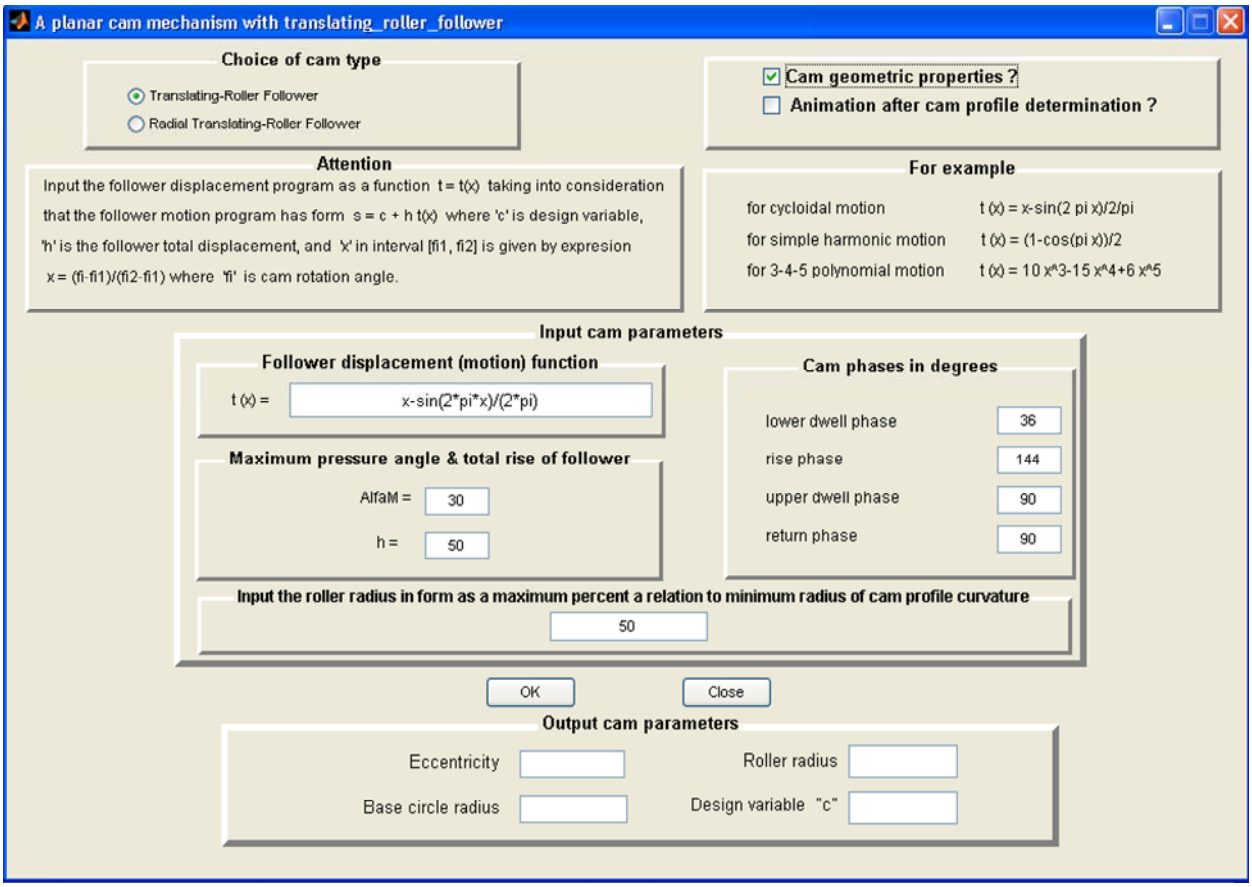

Fig. 4. MATLAB program for cam design optimization

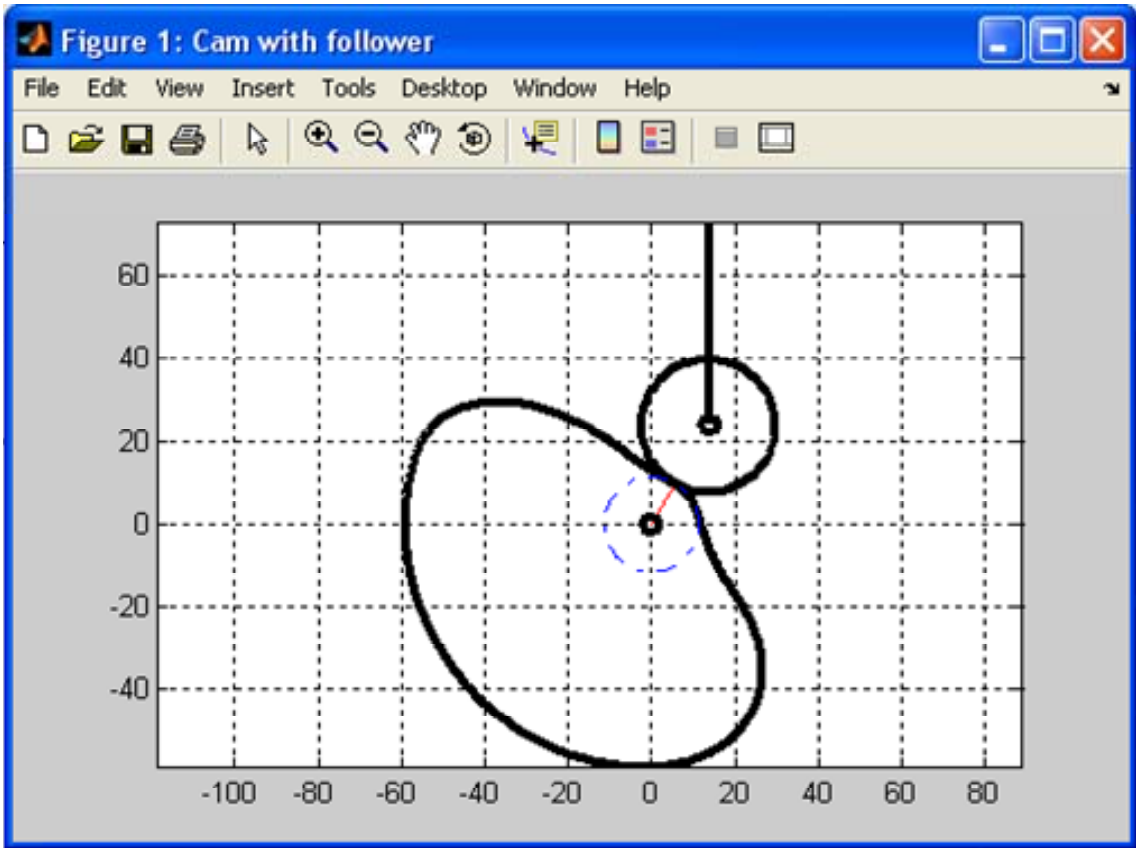

Fig. 5. Determination of the cam profile

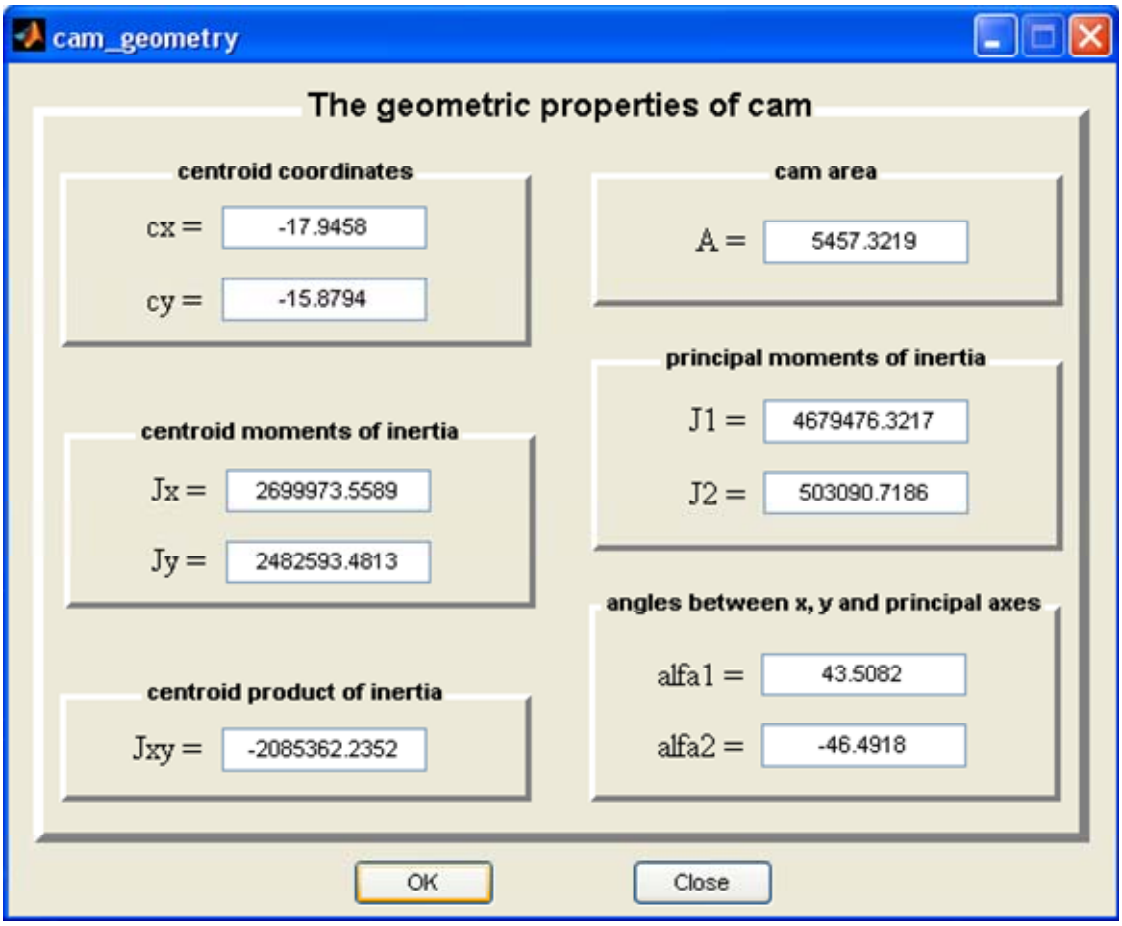

Fig. 6. Determination of the geometric properties of cam

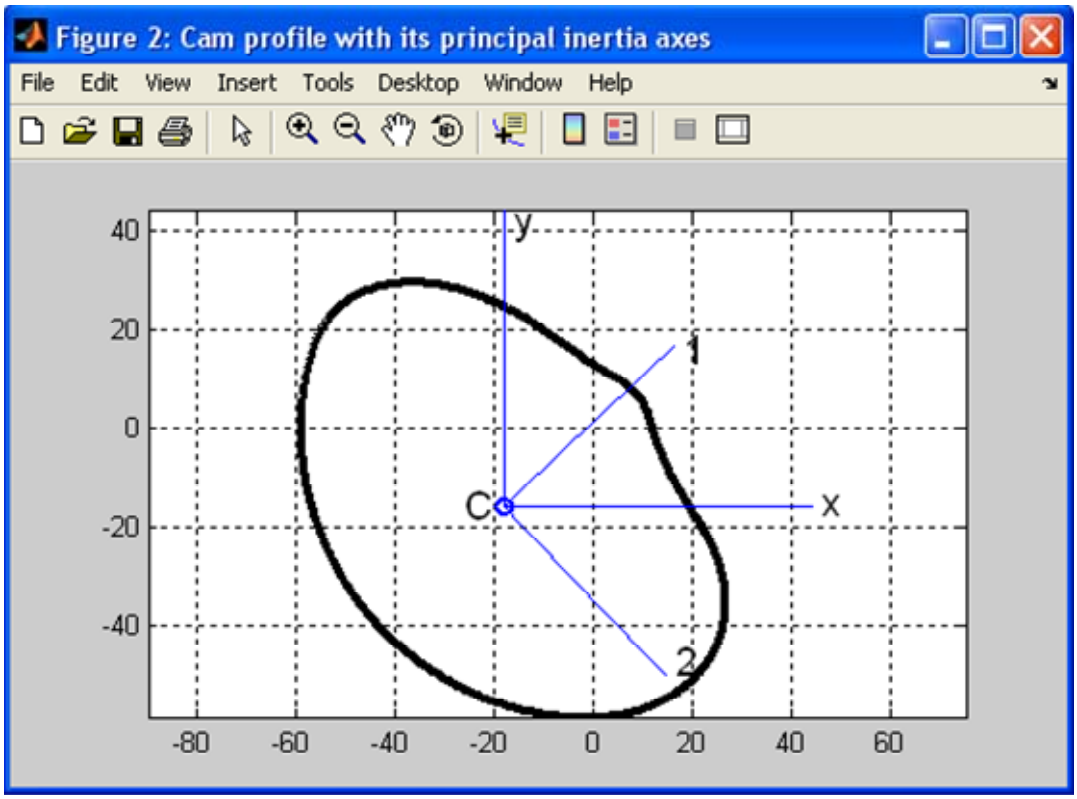

Fig. 7. Principal axes of inertia (1 & 2)

REFERENCES

[1] J. Angeles, C. S. Lopez-Cajun, *Optimization of cam mechanisms.* Kluwer Academic Publishers, 1991.

[2] J. Angeles, C. S. Lopez-Cajun, *Optimal Synthesis of Translating Roller-Follower Cam Mechanisms with Prescribed Functional Constraints*, Tokyo, Japan, 1984, pp. 782–787.

[3] A. Jeffrey, *Mathematics for Engineers and Scientists*, Van Nostrand-Reinhold, London, 1989.

[4] The MathWorks, Inc.: *Matlab, User manual.*

Р е з и м е

ПРОГРАМА MATLAB ЗА ОПТИМИЗАЦИОНА СИНТЕЗА НА РАМНИ БРЕГОВИ МЕХАНИЗМИ СО ТРАНСЛАТОРЕН ЧЛЕН ВОДЕН СО РОЛНА

Даме Коруноски, Иван Мицкоски, Христијан Мицкоски

Машински факултет, Универзитет „Св. Кирил и Методиј“
п. фах 464, МК-1001 Скопје, Република Македонија
dame@mf.edu.mk / ivanm@mf.edu.mk / hristijanm@mf.edu.mk

Клучни зборови: брег; ролна, агол на притисок; matlab (MATLAB)

Предмет на анализа во овој труд е оптимизационата синтеза на рамни брегови механизми со транслаторни членови водени со ролна. Кај овие механизми, клучни параметри на кои треба да се внимава се аголот на притисок и кривината на профилот на брегот. Во трудот е направена програма MATLAB, базирана на „Symbolic Math Toolbox“, која ги пресметува минималниот радиус на основниот круг (минимални димензии на брегот), од аспект на максимален дозволен агол на притисок, и оптималниот радиус на ролната од аспект на одбегнување на феноменот познат како *потсекување*, т.е. од аспект на одбегнување високи контактни напрегања. Влезните параметри се: која било функција која го опишува законот на движење на водениот член, максималниот агол на притисок, одот на водениот член и четири фази: фазата на долно мирување, фазата на подигање, фазата на горно мирување и фазата на приближување. Излезните параметри се: оптимален радиус на основниот круг, оптимален радиус на ролна и профил на брегот. Овозможена е и визуелна графичка презентација на профилот на брегот, пресметка на геометриските карактеристики на брегот, а можна е и анимација на ротацијата на брегот.

Mechanical Engineering – Scientific Journal, Vol. **28**, No. 1, pp. 13–16 (2009)
CODEN: MINSC5 – 402
ISSN 1857–5293
Received: December 15, 2008
UDK: 004.92
Accepted: February 10, 2009

Original scientific paper

PROJECTIONS OF 4D SURFACES

Risto Taševski

Faculty of Mechanical Engineering, SS. Cyril and Methodius University,
P.O Box 464, MK-1001 Skopje, Republic of Macedonia
risto@mf.edu.mk

A b s t r a c t: A geometric and mathematical model, as well as a computer algorithm of 4D surfaces' projections are presented in this paper. The definition of the 4D surfaces' projections is provided by the functions with two variables. 4D surfaces presentation is reduced with presentation of 4D points in 4D geometric space. The points are visible on the display after the transformation in 3D and 2D space. Determined points are connected in the mesh of horizontal and vertical isolines. With the analysis of 4D surfaces the analogy between 3D surfaces and 4D surfaces is confirmed.

Key words: 4D geometry; 4D space; 4D surface

1. 4D POINT

The point is defined with a determined number of coordinates or parameters regarding the space in which it exists. In 1D space the point is determined with one coordinate *A(x)*, in 2D space with two coordinates *A(x,y),* in 3D space with three coordinates *A(x,y,z)*, as well as the point in 4D space is determined with four coordinates *A(x,y,z,w)*. If the point *A* of 4D space *A(x,y,z,w)* is projected in 3D space, 4 projections are obtained on the coordinate hyperplanes *A(x,y,z)*, *A(x,y,w)*, *A(x,z,w)* and *A(y,z,w)* and 6 projections on the coordinate planes *A(x,y), A(x,z), A(y,z), A(x,w), A(y,w)* and *A(z,w)* (Fig.1).

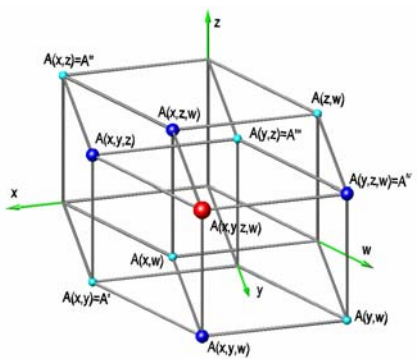

Fig. 1. 4D point

2. 4D SURFACES AND COMPUTER ALGORITHM

4D surfaces are surfaces in which the position of each point is determined with four coordinates. The presentation of 4D surfaces is reduced to the presentation of points in 4D space. 4D point *T(x,y,z,w)* is transformed into 3D and 2D point *T(x,y)* and shown on the screen. For the computer algorithm creation matrices for 4D transformations – scaling, translation and rotation are used.

Matrix for scaling

$$\begin{vmatrix} Sx & 0 & 0 & 0 & 0 \\ 0 & Sy & 0 & 0 & 0 \\ 0 & 0 & Sz & 0 & 0 \\ 0 & 0 & 0 & Sw & 0 \\ 0 & 0 & 0 & 0 & 1 \end{vmatrix},$$

matrix for translation

$$\begin{vmatrix} 1 & 0 & 0 & 0 & 0 \\ 0 & 1 & 0 & 0 & 0 \\ 0 & 0 & 1 & 0 & 0 \\ 0 & 0 & 0 & 1 & 0 \\ Tx & Ty & Tz & Tw & 1 \end{vmatrix},$$

matrix for the rotation around the *xy* plane

$$\begin{vmatrix} 1 & 0 & 0 & 0 & 0 \\ 0 & 1 & 0 & 0 & 0 \\ 0 & 0 & \cos\alpha & -\sin\alpha & 0 \\ 0 & 0 & \sin\alpha & \cos\alpha & 0 \\ 0 & 0 & 0 & 0 & 1 \end{vmatrix}.$$

Matrices for the rotation around other planes, *xz, xw, yz, yw* and *zw,* are obtained with the analogy to the previous.

4D surface is defined by 4D function

$$f(x,y,z,w) = 0,$$

that can be set with 2 variables

$z(x,y) = 0$ and $w(x,y) = 0$,

after that, the coordinates of 4D points *T(x,y,z,w)* could be determined. 4D points are transformed and connected using a simple algorithm:

```
Begin
s1=x2-x1/bragli;
s2=y2-y1/brrad;
   for(i=0; i<s1; i++){
     for(j=0; j<s2; j++){
        function = f(x,y,z,w);
           line(T(x[i],y[j]), T(x[i+1],y[j+1]));
                 }}
end
```

4D points could be connected to a mesh of horizontal (*bragli*) and vertical (*brrad*) isolines. The user interface of the designed computer program provides setting of the border variables $x_1<x<x_2$ and $y_1<y<y_2$ and a coordinate hyperplane in which the projecting would be performed (Fig. 2).

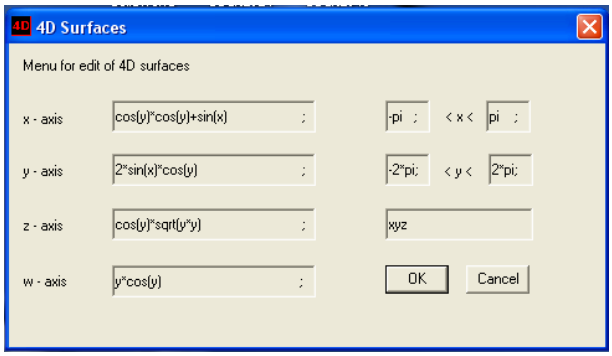

Fig. 2. User interface for setting 4D surfaces

3. THE COMPUTER PROGRAM VERIFICATION

The computer program verification has been performed with setting of simple 2D and 3D structures. The analogy has been performed between 2D structures – parabola, 3D structures – hyperbolical paraboloid and 4D structures – 4D hyperbolical paraboloid.

The basic equation of a parabola is

$$x^2 = 2py\,.$$

If $2p = 1$, then the equation is reduced to $x^2 = y$, from which 2D points are produced.

$$f(x,y,z,w) = (x,x^2,0,0);\ \ x \in R$$

Within the limits $-\pi < x < \pi$ and $-\pi < y < \pi$ the geometric shape on the fFig. 3 is produced.

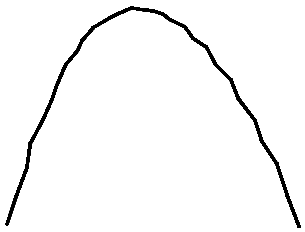

Fig.3. Parabola $f(x,y,z,w) = (x,x^2,0,0)$ for $-\pi < x < \pi$ and $-\pi < y < \pi$

The hyperbolical paraboloid is obtained with sliding of hyperbola along the parabola. This is presented with canonical type of equation as

$$\frac{x^2}{p} - \frac{y^2}{q} = 2z\,.$$

If $p = q = \frac{1}{2}$, then the equation is reduced to $z = x^2 - y^2$ from which 3D points are produced.

$$f(x,y,z,w) = (x,y,x^2 - y^2,0);\ \ x,y \in R$$

Within the limits of $-\pi < x < \pi$ and $-\pi < y < \pi$ the geometric shape of the Fig. 4 is produced.

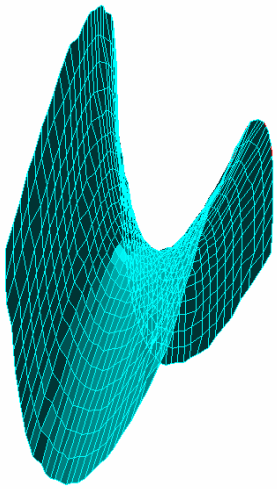

Fig. 4. Hyperbolical parboloid $f(x,y,z,w) = (x,y,x^2 - y^2,0)$ for $-\pi < x < \pi$ and $-\pi < y < \pi$

The projection of the hyperbolical paraboloid on the *xz* coordinate plane is parabola, as well as the projection on the *yz* coordinate plane is hyperbola. According to the analogy, projection of the 4D hyperbolical paraboloid on the *xyz* coordinate hyperplane is hyperbolical paraboloid. That means that *x, y, z* coordinates must have value like the hyperbolical paraboloid has and then the *w* coordinate is added. From this statements the next equation (function) is derived

$$f(x,y,z,w) = (x,y,x^2 - y^2,2xy);\ \ x,y \in R$$

Within the limits of $-\pi < x < \pi$ and $-\pi < y < \pi$ the geometric shape on the Fig. 5 is produced.

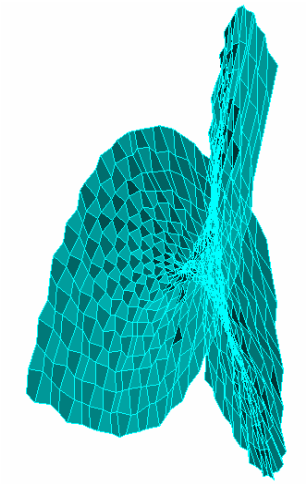

Fig. 5. 4D hyperbolical paraboloid $f(x,y,z,w) = (x,y,x^2 - y^2,2xy)$ for $-\pi < x < \pi$ and $-\pi < y < \pi$

4. GEOMETRIC ANALYSIS OF 4D SURFACES

Geometric analysis is consisted of presentation of the complex 4D surfaces projections on the *xyz* coordinate hyperplane (Fig. 6 – Fig. 9).

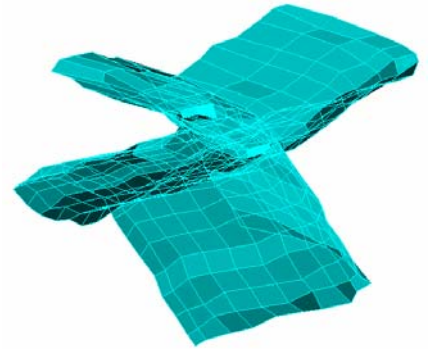

Fig. 6. 4D surface set with function $f(x,y,z,w)=(\sqrt{x^2}, x\cos(x), \sqrt{y^2}, y\sin(y))$ for $-\pi < x < \pi$ and $-\pi < y < \pi$

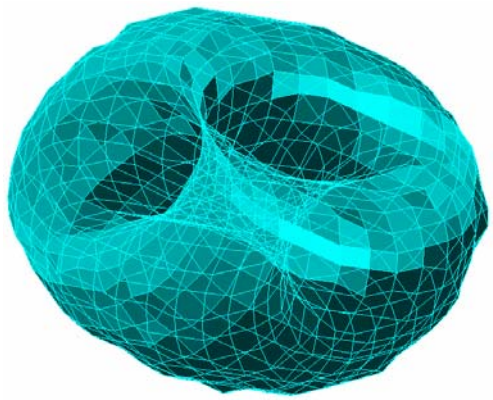

Fig. 7. 4D surface set with the function $f(x,y,z,w) = (\sin(x), \cos(x), \sin(y), \cos(y))$ for $-\pi < x < \pi$ and $-\pi < y < \pi$

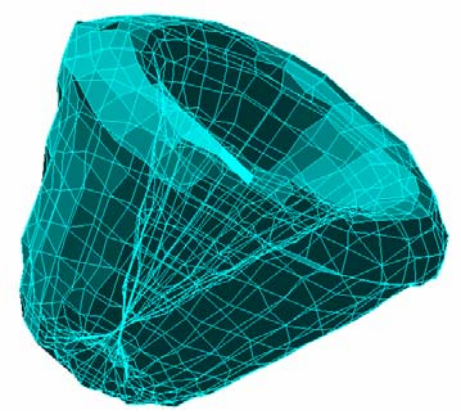

Fig. 8. 4D surface set with the function $f(x,y,z,w) = (x\cos(x), y\sin(x), \sin(y) + \cos(y), \sin(y) + \cos(y))$ for $-\pi < x < \pi$ and $-\pi < y < \pi$

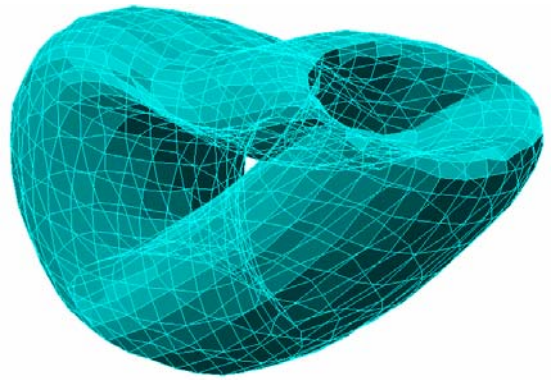

Fig. 9. 4D surface set with the function $f(x,y,z,w) = (\cos(x), \sin(x), \cos(y)\sqrt{y^2}, \sin(y))$ for $-\pi < x < \pi$ and $-\pi < y < \pi$

5. CONCLUSION

The contribution of this paper consists of the way of perception of 4D space. More precisely, 4D surfaces projections are geometrically processed using the function with two variables. The created computer program, based on the presented geometric algorithm, has an ability to analyze the 4D surfaces' projections in an easer and faster way. Verification using analogy has shown that the computer program gives accurate results and can be used for presentation of 4D surfaces.

REFERENCES

[1] T. Banchoff.: *Computer Animation and the Geometry of Surfaces in 3D and 4D Space*, International Congress, Helsinki, 1978, pp.1005–1013.

[2] C. Hinton: *Fourth Dimension*, Kessinger Publishing; Washington, 1997.

[3] H. Manning: *The Fourth Dimension Simply Explained*, Dover Publications, New York, 2005.

[4] В. Филиппов: *Начертательная геометрия многомерного пространства и ее приложения*, Ленинград, 1979.

Р е з и м е

ПРОЕКЦИИ НА 4Д ПОВРШИНИ

Ристо Ташевски

Машински факултет, Универзитет „Св. Кирил и Методиј“
ѝ. фах 464, МК-1001 Скопје, Република Македонија
risto@mf.edu.mk

Клучни зборови: 4Д геометрија; 4Д процтор; 4Д површина

Креиран е геометриски, математички модел и компјутерски алгоритам за претставување на проекции на 4Д површини зададени со функции со две променливи. Претставувањето на 4Д површини се сведува на претставување на 4Д точки во 4Д геометриски простор, имено 4Д-точките се трансформираат во 3Д и во 2Д простор и се прикажуваат на екран. Добиените точки се поврзуваат во мрежа од хоризонтални и вертикални изводници. Извршена е анализа на проекциите на 4Д површини со помош на направена аналогија помеѓу 3Д и 4Д површините.

Mechanical Engineering – Scientific Journal, Vol. **28**, No. 1, pp. 17–25 (2009)
CODEN: MINSC5 – 403
ISSN 1857–5293
Received: March 17, 2009
UDK: 624.078
Accepted: April 27, 2009

Original scientific paper

EXPERIMENTAL ANALYSIS ON THE STRESS DISTRIBUTION OF THE MAIN BEAM ON THE ROOF STRUCTURE IN THE SPORTS HALL IN SKOPJE

Zoran Bogatinoski[1], Vladimir Stojmanovski[2]

[1]*Faculty of Mechanical Engineering, SS. Cyril and Methodius University, P.O Box 464, MK-1001 Skopje, Republic of Macedonia*
[2]*Vivaks Inženering DOO Skopje,*
bogatin@mf.edu.mk, vladimir.stojmanovski@gmail.com

A b s t r a c t: This paper presents the stress and the deformation analysis in the main beam by examining the testing load. The main beams describe the space grid steel beam with a span of 73 meters. The testing has analyzed the behavior of the structure by loading as well as the stress and the deformation in the critical parts of elements. With a purpose to define the loads correctly as their location, the modeling of the structure and computer-numerical simulation with testing load were first finished.

Key words: Carrying roof structure; main space grid girder; modeling; low alloy structural steel; stress analysis; structural testing

1. INTRODUCTION

The testing of the roof structure at the sports hall in Skopje was performed by the joint team of the Faculty of Mechanical Engineering in Skopje and the Faculty of Civil Engineering in Skopje.

The main steel roof structure is a space grid which contains two, main expanse grid steel beams with a spam of 73 m and main plain beams that are put in a square way (Fig. 1).

The main beams are with a free span of app. 73 m and the same are curved with a radius of the curved line R = 174 m, and an arrow of 3.80 m in the middle. The upper and the lower parts are made of warm shaped piped profiles with a squared square area of 400×400×16 and 400×400×20. It's filled (vertical and diagonal) and also is made from warm shaped and piped profiles with a squared cut. The looks of the main beams are shown in the Fig. 2.

The two main beams with a square area of 2,68×5,69 m, are across stiffed 1/3 from the span with three spaced grid bridges in the upper half from the main spaced grid.

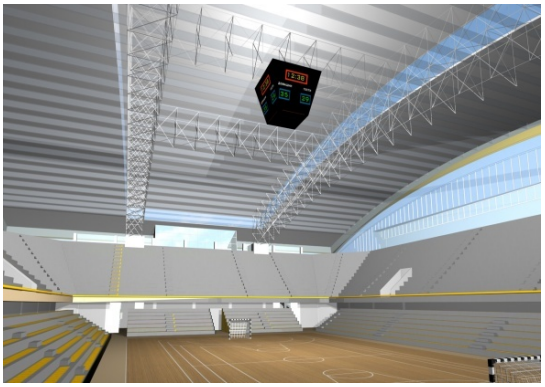

Fig. 1.

Fig. 2

With the project, it is considered that the material for the beams is alloy steel S355J2H (St52-3N) according to EN10210 (DIN 17100), or Č.0563 according to MKS (JUS) C.BO.500.

2. TECHNOLOGY OF MANUFACTURE, PRODUCTION, CONTROL AND TESTING OF THE ELEMENTS AND SEGMENTS OF THE STRUCTURE IN A WORKSHOP AND IN A MONTAGE

Taking this kind "S" of quality and responsibility of the welding structure it is of great importance to finish the analysis that is needed to be done, starting from the phase of fabric production and the work site creating the separate elements, their enlargement, forming the grid beams from the platform in the montage, until their final set of supports.

The testing and the control of the workshop and the montage contain:

– testing the welded joints from the technological rehearses of the welders,
– control of the curved line of the sides in the main beams,
– control of the quality in the surface and corrosion protection in the fabric,
– dimensional control of the square area,
– control of the preparation for the welding of butt and angle welds,
– control of the parameters in the technology of welding,
– control of the order in the realization in the separate welds,
– control of the temperature while heating,
– 100% visual testing and dimensional control of the welds in the separate beams,
– Ultrasound research of the separate welds,
– 100% radiographic control of the butt welds,
– Control of the deformation in the welded elements.

2.1. Enlargement of the main beams at a montage

On the base of the building location a scheme that is curved with the radius in the bend $R = 174$ m and the length equal with the main beams $L = 72.9$ m was made. In that way one flange in the whole length is formed, and it has controlled the position of the different thickness in the square area which represents special importance because it has the same dimensions (400×400 mm), and there is a deference in the thickness (16 and 20 mm).

By welding the curved segments with the length of $L = 8 \div 12$ m enlargement of the beams at the building location is made.

2.2. Welding and enlargement of separate sections of the main space grid beams at a montage

On the base grids (front and back grid) are formed on the main beams. Butts are welded on the flanges, as the angles are welded in the filled (diagonals and verticals) front and back grids, before they are prepared for the montage (connected).

In the Fig. 3 and Fig. 4 the welding on the ground of some welds at separated sections is presented.

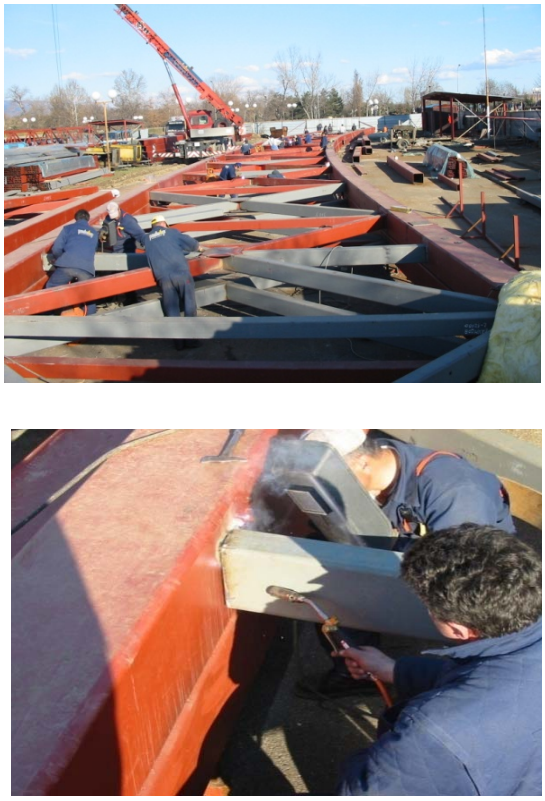

Fig. 3

Because of their large weight and the problems connected to the carrying and the instability, the front and the back grids on the main beams GN1 and GN2 on the first base are made ¼ of the span**.** The formed quarters are transported to the location of the arena of the hall and they enlarged the ½ of the span. The formed halves on the back and the front grids from the beam are lifted and set on the ground from one side and on the auxiliary column that is set in the middle (Fig. 4).

Fig. 4

On the already set front and back halves of the beam, a connection is made by forming the upper and lower horizontal grids. After removing the auxiliary column from the main beam GN2, the look of the beams GN1 and GN2 is showed on the Fig. 5. The main beams GN1 and GN2 are connected to each other horizontally and they are connected to the three space grid structure (bridges) set on a 1/3 of the span as it is showed in the Fig. 5.

Fig. 5

3. MODELING OF THE STRUCTURE AND COMPUTER SIMULATION BY TESTING LOAD ON THE MAIN BEAMS

The structure is modeled with final beam elements by using the computer package SOFISTIK and a computer estimate is made on the main grid beams GN1 and GN2. The testing load for the experimental research is simulated by loading the disposed joints (total 16 joints) from the lower zone.

A computer estimate is made for the 4 phases of loading. Every single phase shows: deflections, static forces and moments and the stress in the separated elements of the structure in the main beams.

Figure 6 shows the behavior of the main beam GN1 (the deformation) for the proper phase of loading.

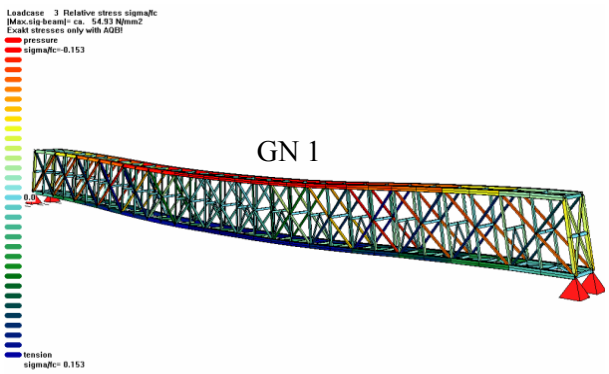

Fig. 6

The largeness of the testing load for the separate phases of analysis in the proper joints (phase 4) is presented in the Fig. 7.

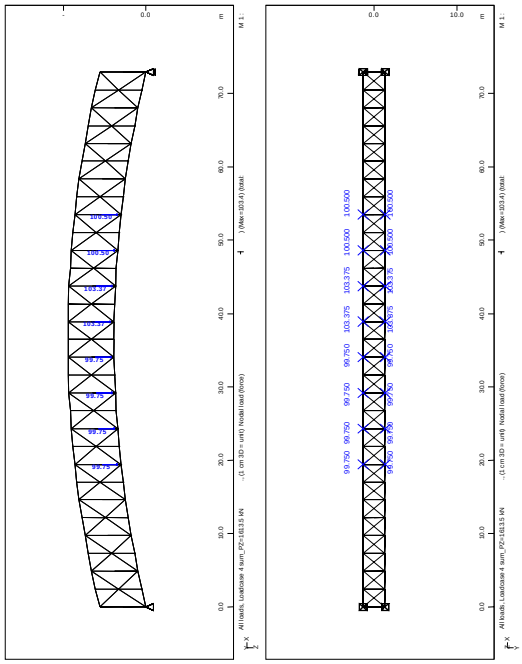

Fig. 7

The diagram in the Fig. 8 presents the largeness of the stress in the separate measurement places (0 to 29) provided by the computer estimate, and in the Fig. 9 the largeness of the deflections of the joints.

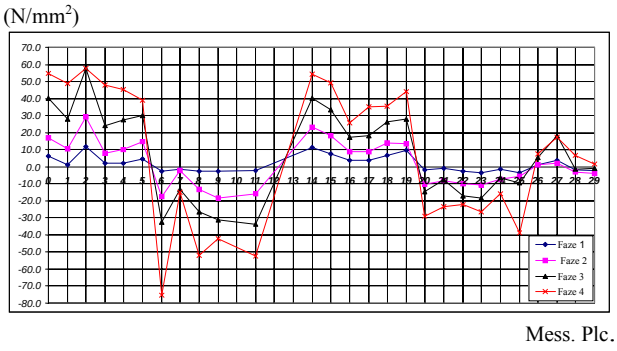

Fig. 8

Theoretic-computer obtained deflections – graphic representation

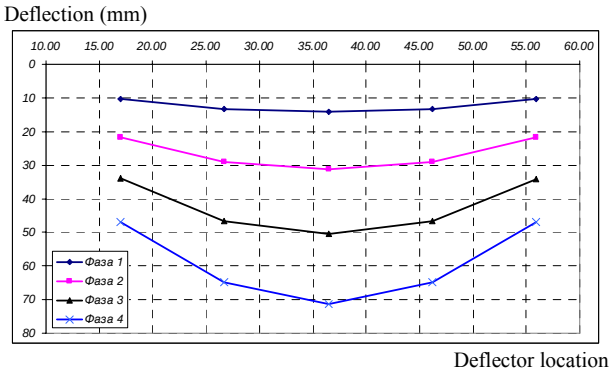

Fig. 9

4. EXPERIMENTAL RESEARCH

4.1. Preparation for the research

The research is done with a purpose to fortify the stressed-deformational condition, as to observe the behavior of the structure under the tested load, in other words the simulated load in the condition of exploitation.

The preparation for the research contains:

1) Production of 4 steel platforms for loading the structure with tested load.

2) Preparation of a steel rope, which is needed to be connected in the prepared ends for hanging on the platform in the defined joints from the lower flange of the structure.

3) To level the platforms, and connect them in the exact place, in the defining joints of the structure after the already done scheme (Fig. 10). Every platform will be hanged in 4 joints from the lower flange of the structure by the steel rope.

4) The total load predicted for the research is 160 t, in other words 40 t per platform. Concrete blocks are used like a load with exact defined weighs and dimensions.

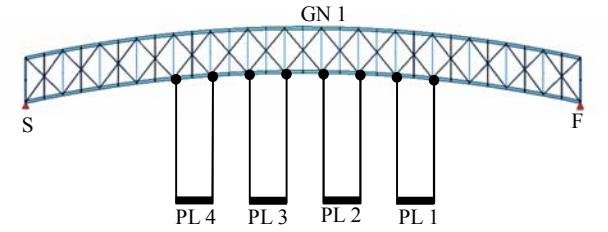

Fig. 10

4.2. Disposition of the measured places

In the research the following parameters were predicted to be measure for:

– horizontal translation in the sliding support (K1, K2, K3),

– vertical deflections in more joints (U1, U2, U3, U4, U5, U6, U7, U8, U9, and U10),

– the measure of the deformations in more points in the elements (sections) of the beam.

The disposition of the parts for measuring the horizontal translation and the vertical deflections are showed in the Fig. 11, and for deformations are showed in Fig. 12.

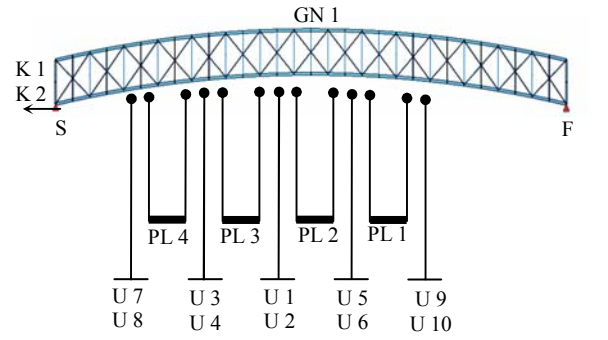

Fig. 11

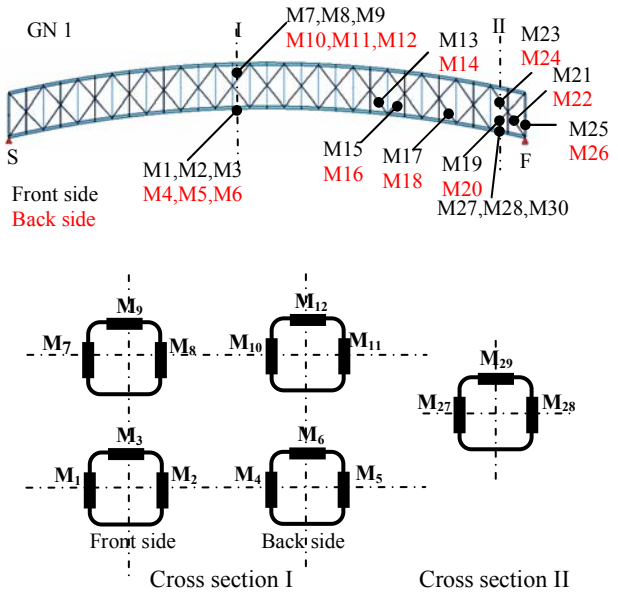

Fig. 12

4.3. The measuring equipment

For measuring the horizontal translation in the sliding support, comparators with precise 0.01 mm are used.

The deflections in the joints are measured with Linear Variable Differential Transducer (LVDT) with precise 0.1 mm.

To measure the deformations in the elements, and estimate the stress in the same parts of the elements, strain gages (SG) which are set in the exact defining parts of the elements are used. The measuring equipment used to determine the deformations is showed in the Fig.13.

For measuring the deformations (stresses) the following measuring equipment is used:

– Strain gages LY21-HBM,

– Wheatstones BridgeUPM60.

Before the beginning of the testing the calibration also known as the proportion of the measure largeness especially for every parts of elements has been confirmed.

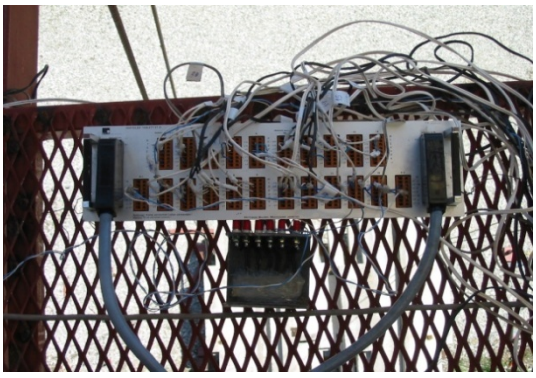

Fig. 13.

4.4. Realization of the research

The measuring of the translation and the deflections in the joints and the deformation in the elements (bars) is realized in few phases in which step by step symmetrically the structure is loaded and unloaded, in other words the beams GN1 and GN2, until it gets the maximal predicted load that is 160 t, by constantly observing the "reaction" of the structure. At the same time the movements in the horizontal (in the sliding support) and the vertical direction (deflections in the joints) are interpreted, like the deformations in the bars in the places of the measuring gages. The order of the total testing load is:

– platform 1 (PL1) 40 200 kg,
– platform 2 (PL2) 40 350 kg,
– platform 3 (PL3) 39 900 kg,
– platform 4 (PL4) 39 900 kg.

In the analysis with the experimental testing load the following phases are predicted:

– 1st phase: 25% from the maximal predicted load (1/2 PL 1 and ½ PL 4) (40150 kg),

– 2nd phase: 50% from the maximal predicted load (PL 1 and PL 4) (80100 kg),

– 3rd phase: 75% from the maximal predicted load (PL 1, 1/2PL 2, ½ PL 3, PL 4) (120425 kg),

– 4th phase: 100% from the maximal predicted load (PL 1, PL 2, PL 3, and PL 4) (160150 kg).

Testing procedure

Fig. 14. Loading platform

Fig. 15. Total load

4.5. The results from the experimental research with the testing load

In the research the following results are obtained:

Beam GN1

– Vertical deflection

	L=	17.01		26.73		36.45		46.17		55.89	
	M.L.	U7	U8	U3	U4	U1	U2	U5	U6	U9	U10
Loading phases	**0**	30	16	27	26	48	14	90	39	4	21
	1	33	19	30	29	52	17	94	42	8	25
		3	3	3	3	4	3	4	3	4	4
		3		**3**		**4**		**4**		**4**	
	2	43	28	42	42	66	31	107	54	17	34
		13	12	15	16	18	17	17	15	13	13
		13		**16**		**18**		**16**		**13**	
	3	53	39	59	58	84	47	123	70	28	44
		23	23	32	32	36	33	33	31	24	23
		23		**32**		**35**		**32**		**24**	
	4	67	58	78	77	105	69	142	89	41	57
		37	42	51	51	57	55	52	50	37	36
		40		**51**		**56**		**51**		**37**	

L (m) – Distance between support and node
ML – Measuring location

	Average value of the deflection obtain by easurement				
	M.M	U7/U8	U3/U4	U1/U2	U5/U6	U9/U10
	L=	17.01	26.73	36.45	46.17	55.89
Loading phases	**1**	3	3	4	4	4
	2	13	16	18	16	13
	3	23	32	35	32	24
	4	40	51	56	51	

The obtained results of the deflection for the separated phases of the research are presented graphically on the Fig. 16.

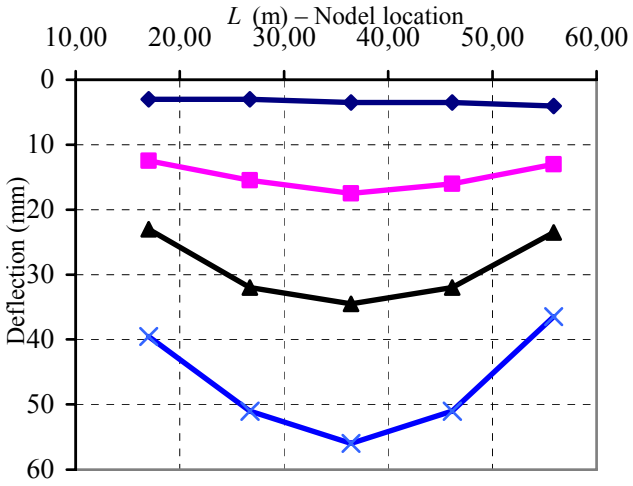

Fig. 16. The change of the deflection under different length parts of the beam for different phases

– Horizontal translation in the sliding support

Loading phases	K_1 (mm)	K_2 (mm)
1	0.8	1
2	8	7,2
3	16	15
4	25	23

K_1 – translation into the left sliding support
K_2 – translation into the right sliding support

Real deformations and stresses in some parts of the elements:

		0	**1**	**2**	**3**	**4**	**5**	**6**	**7**	**8**	**9**	**11**	**14**
Phase 1	e_o	-1	-3	5	-3	-2	-1	0	1	2	-2	0	-12
	e	28	2	62	7	8	20	-12	-6	-11	-15	-11	43
	De	29	5	57	10	10	21	-12	-7	-13	-13	-11	55
	σ	6,1	1,1	12,0	2,1	2,1	4,4	-2,5	-1,5	-2,7	-2,7	-2,3	11,6
Phase 2	e_o	-1	-3	5	-3	-2	-1	0	1	2	-2	0	-12
	e	80	47	144	34	47	69	-84	-10	-62	-90	-75	99
	De	81	50	139	37	49	70	-84	-11	-64	-88	-75	111
	σ	17,0	10,5	29,2	7,8	10,3	14,7	-17,6	-2,3	-13,4	-18,5	-15,8	23,3
Phase 3	e_o	-1	-3	5	-3	-2	-1	0	1	2	-2	0	-12
	e	190	130	280	111	129	142	-154	-63	-124	-151	-161	180
	De	191	133	275	114	131	143	-154	-64	-126	-149	-161	192
	σ	40,1	27,9	57,8	23,9	27,5	30,0	-32,3	-13,4	-26,5	-31,3	-33,8	40,3
Phase 4	e_o	-1	-3	5	-3	-2	-1	0	1	2	-2	0	-12
	e	260	229	279	225	214	184	-359	-71	-245	-203	-249	246
	De	261	232	274	228	216	185	-359	-72	-247	-201	-249	258
	σ	54.8	48,7	57,5	47,4	45.4	38.9	75.4	-15.1	-51.9	-42.2	-52.3	54.2

		15	16	17	18	19	20	21	22	23	24	25	26	27	28	29
Phase 1	e_o	-11	-5	-6	-5	-19	-3	-5	-2	2	-4	-12	-2	12	6	4
	e	24	12	11	26	26	-12	-10	-14	-15	-10	-29	3	29	-2	-6
	De	35	17	17	31	45	-9	-5	-12	-17	-6	-17	5	17	-8	-10
	σ	7,4	3,6	3,6	6,5	9,5	-1,9	-1,1	-2,5	-3,6	-1,3	-3,6	1,1	3,6	-1,7	-2,1
Phase 2	e_o	-11	-5	-6	-5	-19	-3	-5	-2	2	-4	-12	-2	12	6	4
	e	76	36	35	62	45	-53	-44	-49	-50	-38	-39	4	22	-9	-14
	De	87	41	41	67	64	-50	-39	-47	-52	-34	-27	6	10	-15	-18
	σ	18,3	8,6	8,6	14,1	13,4	-10,5	-8,2	-9,9	-10,9	-7,1	-5,7	1,3	2,1	-3,2	-3,8
Phase 3	e_o	-11	-5	-6	-5	-19	-3	-5	-2	2	-4	-12	-2	12	6	4
	e	149	78	80	119	113	-72	-41	-83	-85	-35	-58	24	99	-1	0
	De	160	83	86	124	132	-69	-36	-81	-87	-31	-46	26	87	-7	-4
	σ	33,6	17,4	18,1	26,0	27,7	-14,5	-7,6	-17,0	-18,3	-6,5	-9,7	5,5	18,3	-1,5	-0,8
Phase 4	e_o	-11	-5	-6	-5	-19	-3	-5	-2	2	-4	-12	-2	12	6	4
	e	224	117	162	165	191	-141	-116	-107	-125	-80	-197	33	94	38	12
	De	235	122	168	170	210	-138	-111	-105	-127	-76	-185	35	82	32	8
	s	49,4	25,6	35,3	35,7	44,1	-29,0	-23,3	-22,1	-26,7	-16,0	-38,9	7,4	17,2	6,7	1,7

e_o – deformation in zero position
e – measured deformation in phases
$De = e - e_o$
$\sigma = E \cdot \varepsilon$ (N/mm^2)

When you take in place the characteristics of the strain gages, the measuring base and the module of the elasticity it obtains K=0.21 which can count the obtained deformation that is used to get the stress.

For an example of SG16 in phase 4:

$$\sigma = K\varepsilon = 0.21 \cdot 122 = 25.6 \ \text{N/mm}^2 .$$

5. THE COMPARED ANALYSIS AND THE REVIEW OF THE OBTAINED RESULTS FROM THE THEORETIC AND EXPERIMENTAL RESEARCH

Next are the tabular and the diagram presentation of the obtained (theoretic and experimental) largeness of the deflection in several joints from the beam, the horizontal movements in the sliding support, the same is with the stress in the separated bars from the main beams GN1 and GN2, and with their comparable analysis that is picturesque and simple to get to the conclusion for the theoretic and experimental response and the behavior of the beams under the action from the testing loads which are needed to be transferred over the beams into the reinforced concrete columns to the concrete fundaments.

The main beam GN1

AVERAGE VALUE OF MEASURED DEFLECTION					
M.M	U7/U8	U3/U4	U1/U2	U5/U6	U9/U10
L =	17.01	26.73	36.45	46.17	55.89
1	1	3	4	4	4
2	13	16	18	16	13
3	23	32	35	32	24
4	40	51	56	51	37
TEORETICAL DEFLECTION					
1	10	13	14	13	10
2	22	29	31	29	22
3	34	47	50	47	34
4	47	65	71	65	47
TOLERANCE (%)					
4	15.6	21.4	21.4	21.5	22.1

The average values of the already measured deflection in the separated joints, are received theoretically and experimentally in the experimental loading and they are given in the Fig.17 and Fig.18.

The obtained theoretic values for the deflections are bigger than the deflections received from the experimental research. The deviations are in the zone from 16 to 22 %.

The distance – the positi on of the LVDT

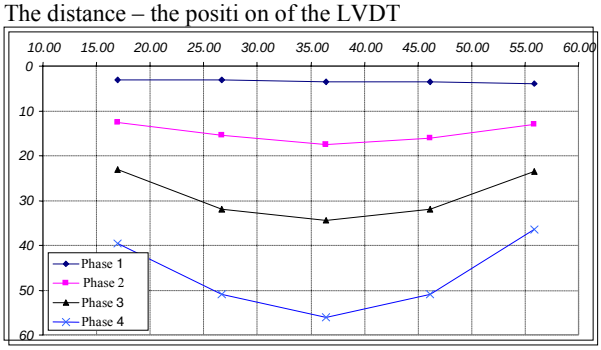

Fig. 17. Experimental deflections from the testing loading

The distance - the position of the LVDT

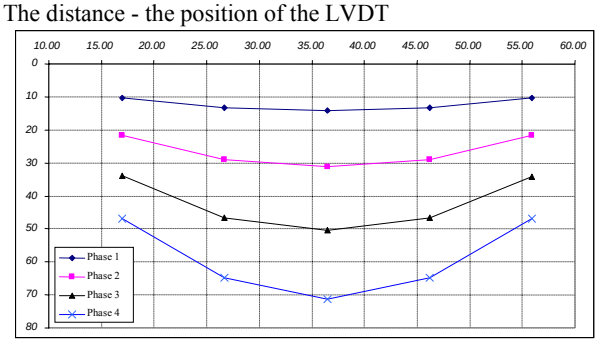

Fig. 18. Theoretic deflection from the simulation of the testing loading

The average values of the horizontal translation on the sliding support are provided experimentally and theoretically and they are showed in a table and in a graph.

Horizontal translation GN1

	Horizontal translation					
	Experimental values			Theoretic values		
M.M	K1	K2	S.V.	K1	K2	S.V
Phase	mm	mm	mm	mm	mm	mm
1	0.8	1	0.9	7.02	7.02	7.02
2	8	7.2	7.6	15.06	15.06	15.06
3	16	15	15.5	23.91	23.91	23.91
4	25	23	24	33.114	33.114	33.114

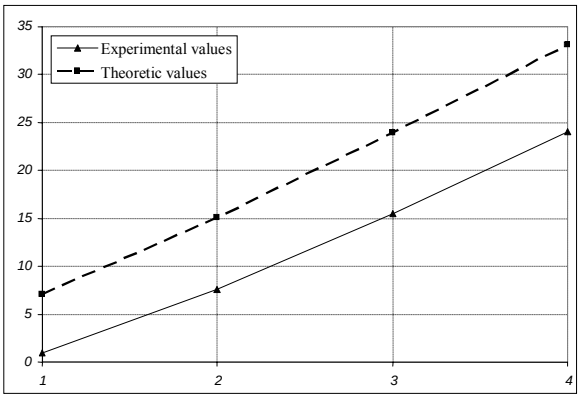

Fig.19. Translation in the sliding support for different phase of loading

For every single strain gage the theoretic and experimental values of the stress for the separated phases of the loading are showed graphically:

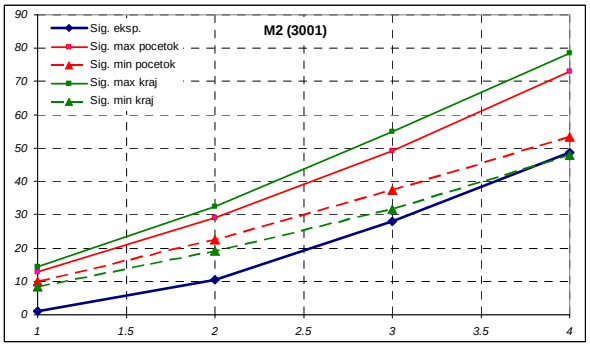

Fig. 20. Theoretic and experimental values for the stress in SG2

The legend is related to all of the strain gages (from SG1 to SG30) and the appropriate bars in which the measuring places are set.

From the entire previous presentation, it can be concluded that the accomplished values for the translations, deflections and the stresses from the theoretic analysis, compared with those from the experimental research in an enormous amount are coincided. Concessions are in allowed and expected areas.

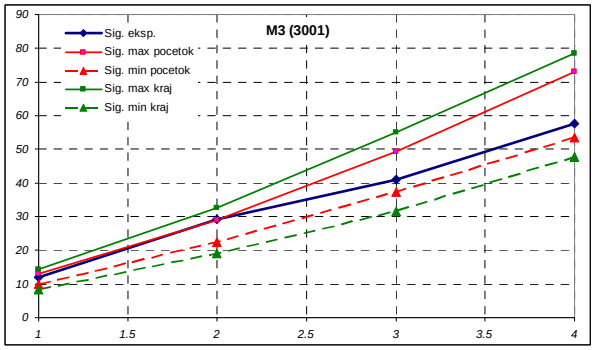

Fig. 21. Theoretic and experimental values for the stress in SG3

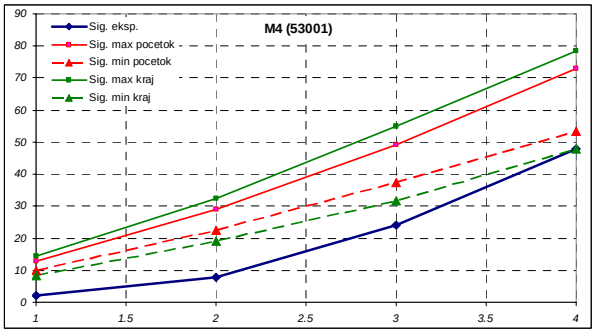

Fig. 22. Theoretic and experimental values for the stress in SG4

6. CONCLUSION

On the base on the complete theoretic and experimental researches, as the complete analysis on the obtained results it can be considered and concluded the following:

– The maximum stress in the elements of the structure in the worst combination of loads (1+2+3+4), which rarely can happen, is 195.1 N/mm^2. And it is known under the allowed stress.

– Because it is about an incredible responsible structure, with a permission that is taking place, a research on the structure with an experimental loading is complete. A load which amounts 80% from the projected maximum load is simulated on the structure.

– A mathematical model of the structure is complete and the experimental load for every single phase of loading is simulated in separated joints.

– The results are got with a theoretical and experimental research and they are enormously coincided.

– In the research with the experimental loading it is not noticed the compliance in any of the elements of the structure.

– On the basis of the research of the material, the research for confirming the technology of the

welding, the research for the welded joints and connections and the research with the experimental load, it can be concluded that the structure is made excellent and in total it has the requirement for the "S" ("B") category of quality of the welded connections as the request for the important standards from this division.

– The completed knowledge from the research has big importance for the metal industry in R. Macedonia and for the experts, the architects, the mechanical and the civil engineers who work in area of the steel structures.

REFERENCES

[1] "Извештај за извршено испитување со пробно оптоварување на главните просторно решеткасти носачи GN1 и GN2 од носечката покривна челична конструкција на објектот Повеќенаменска и спортска сала на град Скопје". Машински факултет Скопје, 2006.

[2] V. Stojmanovski: *Research in the field of welding, control and testing of carrying roof structure made of low alloy steel for multy purpose sport hall of the city of Skopje,* Master thesis, Faculty of Mechanical Engineering, Skopje, 2006.

[3] Z. Bogatinoski: *Numerical modeling and experimental analyses of the composite steel frames*, Doctoral thesis, Faculty of Mechanical Engineering, Skopje, 2000.

Р е з и м е

ЕКСПЕРИМЕНТАЛНА АНАЛИЗА НА НАПОНСКАТА СОСТОЈБА НА ГЛАВНИТЕ НОСАЧИ НА ПОКРИВНАТА КОНСТРУКЦИЈА НА СПОРТСКАТА САЛА ВО СКОПЈЕ

Зоран Богатиноски[1], Владимир Стојмановски[2]

[1] *Машински факултет, Универзитет „Св. Кирил и Методиј" п. фах 464, МК-1001 Скопје, Република Македонија,*
[2]*Вивакс Инженеринг ДОО Скопје*
bogatin@mf.edu.mk // vladimir.stojmanovski@gmail.com

Клучни зборови: Носечка покривна конструкција; главен просторен решеткаст носач; моделирање; нисколегиран конструктивен челик; анализа на напони; испитување со пробно оптоварување

Во трудот е прикажана анализата на напоните и деформациите во главните носачи при испитување со пробен товар. Главните носачи претставуваат просторно решеткасти челични носачи со распон од 73 метри. При испитувањето е определен однесувањето на конструкцијата при оптоварување како и напоните и деформациите во критичните места. Со цел правилно да се дефинираат товарите, како и нивната локација, претходно е извршено моделирање на конструкцијата и компјутерска симулација при оптоварувањето со пробен товар.

Mechanical Engineering – Scientific Journal, Vol. **28**, No. 1, pp. 27–30 (2009)
CODEN: MINSC5 – 404 ISSN 1857–5293
Received: March 24, 2009 UDK: 621.778
Accepted: April 8, 2009

Original scientific paper

INVESTIGATIONS OF INFLUENCE FACTORS IN THE PROCESS OF THE WIRE DRAWING

Igor Lazarev, Jasmina Čaloska, Atanas Kočov

Faculty of Mechanical Engineering, SS. Cyril and Methodius University,
P.O Box 464, MK-1001 Skopje, Republic of Macedonia
igorspm@yahoo.com

A b s t r a c t: This paper presents the analysis of the wire drawing process by using analytical methods which have been confirmed with the Finite Element Analysis. Also, the point of interest in this paper was the influence of the friction. The optimal friction that can insure minimum force for the wire drawing process has been defined.

Key words: wire drawing; die; stress-strain condition; friction; lubrication

BASIC CHARACTERISTICS OF THE PROCESS OF WIRE DRAWING AND INFLUENCE FACTORS

Cold drawing is the term applied to a range of cold working finishing involving thin rod, wire, extruded tube or sheet metal. Cold drawing of rod, wire and tube may be considered to be the opposite of direct extrusion in the material stock which is pulled through a die rather than pushed through it. As with all cold working processes, work hardenings occur and the grain flow in the finished product runs in the direction of working. Namely, wire drawing is a process where the circular wire is produced by cold drawing and involves pulling material through a tapered die to reduce the diameter from d_0 to d_1 (Fig. 1). While the process of wire drawing is running, three characteristic die sectors are formed in the material.

Sector I is the entrance of the material with the initial diameter d_0. In the case where the process is running without opposite forces, the stresses are not appeared in the material. Sector II is the main sector of the plastic deformation process where the material-wire changes the cross section area and 3D stress condition appears. Sector III is the part where the material is in front of the die exit and linear stress condition is present. The material is under the elastic deformation stress condition.

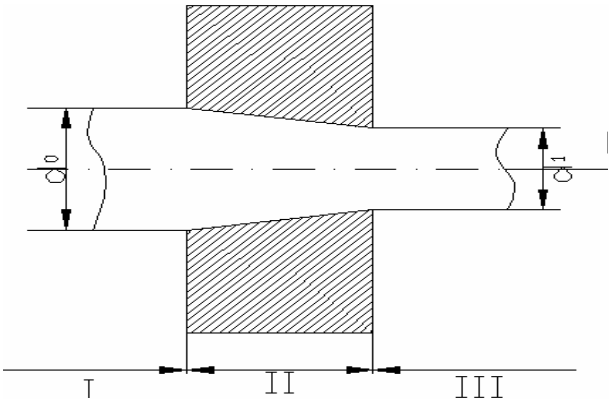

Fig. 1. Sections of the die for the wire drawing process

INFLUENCE OF THE CONTACT FRICTION TO THE PROCESS OF WIRE DRAWING

Forces of the contact friction are necessary to be put on minimum degree due to their handicap of the wire drawing process. That is achieved with previous dressing of the surface of material, with the use of lubricants and securing condition for liquid friction. Liquid friction rests on activity and viscosity of lubricant, from conditions of its intake, also from the speed of drawing, design of the die and temperature in the deformation zone.

During the entrance of die, penetration of the liquid in the zone of deformation can be handicap because of high pressure over the material.

Conditions when the diameter is increasing relating deformations resistance and lubrication are worst because in that sector stress condition with three axis pressure ($\sigma_r<\sigma_\theta<\sigma_x<0$) appears.

According to these conditions, to satisfy the terms of plasticity, the equation must be valid:

$$\sigma_r - \sigma_x = -\sigma_s \qquad (1)$$

The radial stress σ_r can significantly excel the real stress σ_s. Subsequently, significantly are obstructing the conditions of penetrating the lubricant in drawing die. During the usual process of drawing the lubricant is inflicting on the surface of material on a method of adhesion. In relations with the described condition, the lubricant layer is attenuate in the entrance of die, and on many points is braking, therefore friction is going on a border layer or on dry (Fig. 2).

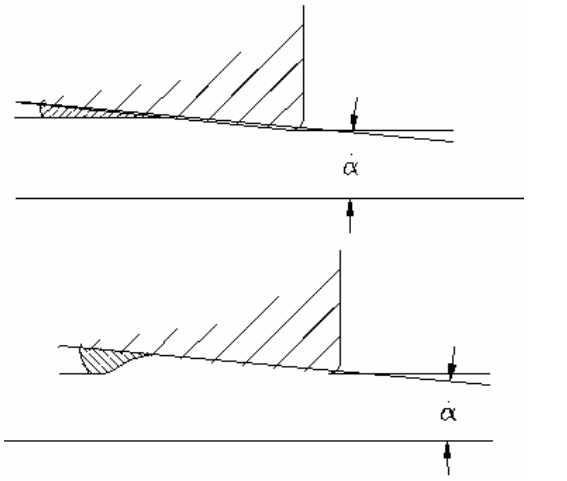

Fig. 2. Lubrication in the deformation zone

With the enlargement of the dies angle, the conditions of lubrications are degrading because of increasing the possibility for collapsing the lubricant layer.

In order to improve the friction conditions, thereby to lower the resistance and increase the speed of drawing, practicing duress importing of lubricant in to the die. For that purpose two methods are worked out: hydrostatic and hydrodynamic. Sometimes, they are used in combination.

Increased viscosity of the lubricant degrades its removal from the surface of the drawn material, but therefore it improves the conditions of entry in die. In addition to certain point the resistances are increased, thereby the drawing force is increased. Therefore very often lubricants with a small coefficient of viscosity are used and with high adhesion power, specially during drawing of thin wall tube, where even small variations of drawing force can prejudice the process of wire drawing.

While selecting the lubricant, besides the known influences, it is necessary to look after the lubricant not to create chemical connections with the drawing material or the die, to satisfy the basic hygienic-technical needs and not to leave marks on the surface of the drawn material.

The best lubricant effect is reached during complete liquid friction. But because of complications to simultaneously satisfy all needs, not every time that kind of conditions can be create. Therefore, in many cases conditions of limit friction must be tried to apply, respectively creating a monomolecular lubricant layer on the contact surface, well agglutinative on the drawing material.

A layer like that can be created from absorb soup layer which is formed on the surface of the drawing material, while friction with lubricant that concerns a certain value on the surface active materials like salts of fat acids, components of chlorine, sulfur and others.

CORRELATIONS BETWEEN DRAWING FORCE AND FRICTION

For the analysis of the process of the drawing wire we use low carbon steel Č.0271 with an initial diameter of ϕ 5 mm which we reduce to the diameter of ϕ 4.45 mm. First, we calculate the optimal angle according to the empire expression after Zibel:

$$\alpha_{\text{opt}} = \sqrt{\frac{\mu \ln\left(\frac{d_0}{d_1}\right)^2}{C}} = \sqrt{\frac{0.1 \ln\left(\frac{5}{4.45}\right)^2}{0.67}} = 0.21 \text{ rad}, \tag{2}$$

or

$$\alpha_{\text{opt}} = 12°.$$

INVESTIGATION OF THE OPTIMAL ANGLE BY USING ABAQUS FEA

The models of die and wire are drawn in an axisymmetric two-dimensional projection, that secures increase of the speed and efficiency of the simulations and determinations.

If the input values in the ABAQUS FEA for steel Č.0271 are:

$E = 210.000$ N/mm^2,

$\mu = 0.3$,

$\rho = 7500$ kg/m^3,

plasticity =

Data

	Yield Stress	Plastic Strain
1	392	0
2	401	0.11
3	409	0.12
4	461	0.19
5	487	0.24

.

Then the models are shown in the assembly, discretization and at the end boundaries and displacement (Fig. 3):

- die boundary to *y*-axis,
- wire boundary to *x* and *z*-axis,
- wire is given displacement to the negative *y*-axis.

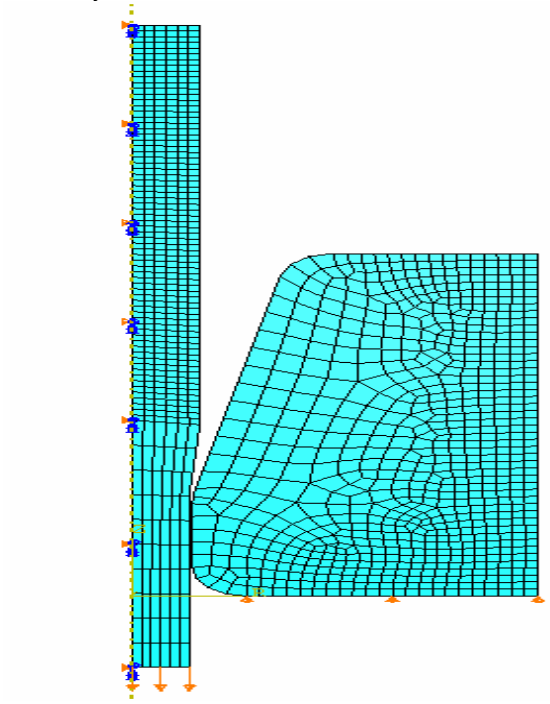

Fig. 3. Given boundaries and displacement

Results which are obtained from the analysis by using FEM could be presented as they are shown on Fig. 4 for the real stresses.

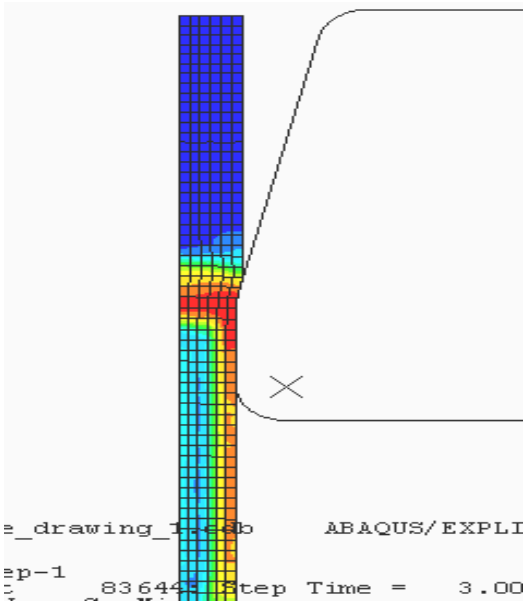

Fig. 4. Real stress in the wire drawing process of ϕ 5.0 mm→ϕ 4.45 mm

By using ABAQUS FEA we can understand the influence of friction on the drawing force, respectively how the force is changing, when using different values of friction for the same type of material, using the same degree of reduction, during drawing with the same die angle. On Fig. 5 is shown the drawing force using friction $\mu = 0.02$

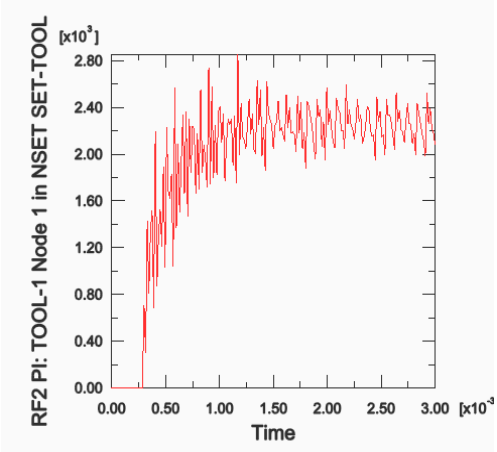

Fig. 5. Drawing force using friction $\mu = 0.02$

The second case shows the drawing force using friction $\mu = 0.06$ (Fig. 6).

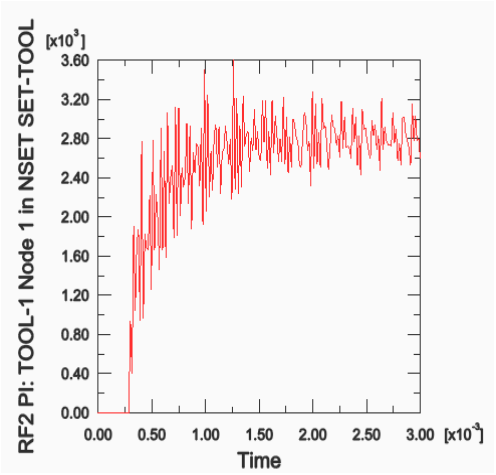

Fig. 6. Drawing force using friction $\mu = 0.06$

The third case shows the drawing force using friction $\mu = 0.1$ (Fig. 7).

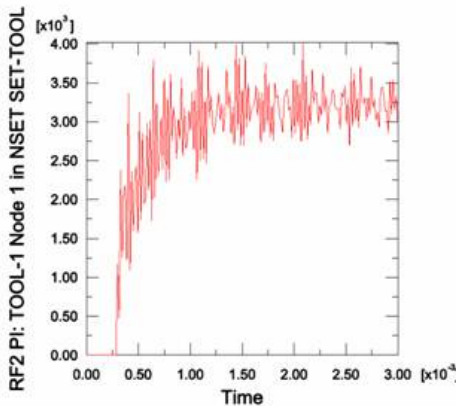

Fig. 7. Drawing force using friction $\mu = 0.1$

The fourth case shows the drawing force using friction $\mu = 0.14$ (Fig. 8).

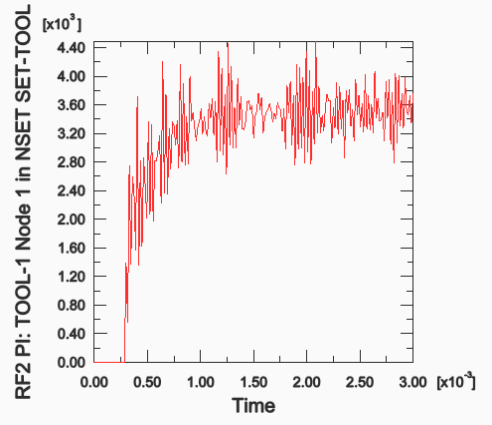

Fig. 8. Drawing force using friction $\mu = 0.14$

Based on the four cases described above, the diagram could be drawn to present the changes of drawing force according to friction (Fig. 9).

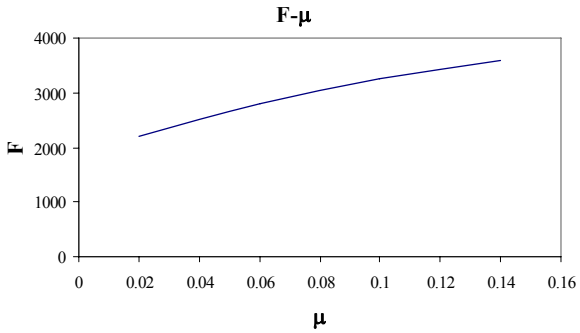

Fig. 9. Influence of friction on the drawing force

By observing the diagram (Fig. 9) it can be confirmed that the drawing force is increasing proportionally with increasing the friction. But when the force is increasing, the axial stress on the exit of die is also increasing; thereby the danger of lacheration of wire is very high. Also, this means bigger consumption of electricity.

CONCLUSIONS

Friction is a very important element in the wire drawing process. The intension of the process is to have minimum of friction, because it leads to achieving minimum drawing force, therefore minimum consumption of electricity. To insure the minimum friction during the process of wire drawing the constructor must look for selection of lubricant, selection of die, quality of surface of the drawing wire, degree of reduction and temperature in the deformation zone.

REFERENCES:

[1] B. Muzafija, *Plastic deformation processing of metals*, Svjetlost, Sarajevo, 1988.

[2] M. Pešiš, *Cold wire drawing*, Zagreb, 1977.

[3] J. Lazarev, V. Strezov, *Machines and deformation processing*, University St. Cyril and Methodius, Skopje, 1987.

[4] B. Devendžić, *Plasticity and deformation processing of metals*, Scientific Book, Belgrade, 1992.

[5] Lj. Dudeski: *CAE – Computer Aided Engineering*, University St. Cyril and Methodius, Skopje, 1996.

[6] I. L. Perlin, M. Z. Ermanok, *Theory of drawing*, Moscow 1971.

[7] J. Lazarev: *Technology of deformation processing*, University St. Cyril and Methodius Skopje.

[8] V. Strezov, *Deformation processing*, University St. Cyril and Metodius, Skopje 1993.

[9] V. Strezov, *Technology of deformation processing*, University St. Cyril and Metodius, Skopje.

[10] I. L. Perlin, L. H. Raitbarg, *Theory of forging metals*, Moscow, 1975.

[11] ABAQUS, User Manual.

Резиме

ИСТРАЖУВАЊЕ НА ВЛИЈАТЕЛНИ ФАКТОРИ ПРИ ПРОЦЕСОТ НА ВЛЕЧЕЊЕ ЖИЦА

Игор Лазарев, Јасмина Чалоска, Атанас Кочов

Машински факултет, Универзитет „Св. Кирил и Методиј“,
п. фах 464, 1000 Скопје, Република Македонија
igorspm@yahoo.com

Клучни зборови: влечење жици; матрица; напонско-деформациска состојба; триење; подмачкување

Во овој труд се претставени анализи на процесот на влечење жица со употреба на аналитички методи кои што се потврдени со метод на конечни елементи. Предмет на интерес во овој труд е и влијанието на триењето. Оптималното триење при процесот на влечење жица може силата на влечење да ја сведе на минимум.

Mechanical Engineering – Scientific Journal, Vol. **28**, No. 1, pp. 31–34 (2009)
CODEN: MINSC5 – 405 ISSN 1857–5293
Received: Octobrr 2, 2009 UDK: 621.833
Accepted: March 18, 200?

Professional paper

JUSTIFICATION ANALYSIS OF UNIVERSAL GEAR REDUCER ASSORTMENT EXTENSION

Siniša Kuzmanović[1], Petar Simonovski[2]

[1]*Faculty of Technical Sciences, Trg Dositeja Obradovića 6, Novi Sad, R. Serbia*
[2]*Faculty of Mechanical Engineering, SS Cyril and Methodius University, P.O Box 464, MK-1001 Skopje, Republic of Macedonia*
kuzman@uns.ns.ac.yu // pero@mf.edu.mk

A b s t r a c t: This paper examines the issue of the universal gear reducer assortment extension of the existing product lines. It is well known the rigorous producer competition on the universal gear reducer market. Also, a bigger part of the producers is trying to extend their assortment in order to satisfy the market's needs. This paper offers some solutions in resolving this issue.

Key words: analyses; assortments; universal; gear reducer

1. INTRODUCTION

The assortment of the products varies in respect to the producer, the seller, and the customer. The assortment of the products in respect to the producer is the smallest of the three since the producer always wants to cut operating costs where as the market demand forces them to expend the variety of the products. The assortment of the seller is usually the biggest since they sell products from different producers. The assortment of the customer is the smallest, but this is not a rule.

PROBLEM DESCRIPTION

The assortment of the products, in this case the universal gear reducer, represents all universal gear reducers that specific producer manufactures and offers to the market. One should recognize several aspects of the product assortment: width of the assortment (number of different types of reducers), length of the assortment (number of different types of reducer of the same type of reducer), height of the assortment (number of different variants in scope of the same dimension – with foot, flange, small flange), and the so called *n*th dimension assortment (connection with a special or regular electric motor, connection with an inlet sub connector, etc.). Producers of universal reducers copy the technical specifications of the leading world producers mainly the SEW company, since current standards do not define the technical specifications of universal reducers. Therefore, the leading world producers' standards are accepted as their own, "internal" standard. On the other hand, some smaller producers are trying to find gaps in the product offer of the bigger producers, and gain customers with reducers that are not offered in the current "standards". This paper concentrates only on the analyses of the universal gear reducer's axis heights.

BASIC CHARACTERISTICS OF AXIS HEIGHTS

Recommended numbers are from the standard line R20 for the universal reducer's axis heights. However, almost all producers use the less dense line R20/2 or R10 since R20 is highly dense and therefore more expensive. This comes from the great number of different tools and a great number of components which is needed to be stored. This approach is completely justified since the axis height growth factor fits into the rotation moment (q_T) growth factor whose value comes out of the regular values of f_B (Fig. 1).

One can see from Fig.1 the areas of the optimal use of universal gear reducers.

Selection of the reducer is done by the following formula:

$$T_N \geq K_A T_i \,. \qquad (1)$$

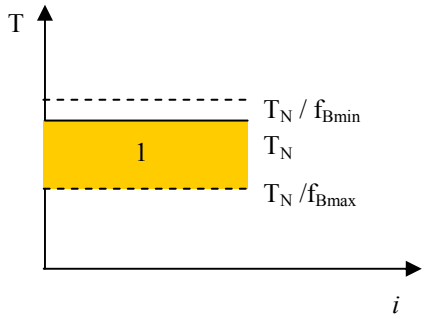

Fig. 1. Graphical interpretation of the optimal usage area of universal gear reducer (1 – area reducer optimal usage)

Where is: T_i – output torque, K_A – application factor whose value limits usually

$$1{,}0 \le K_A \le 2.25\,. \tag{2}$$

Similarity theory:

$$q_h = \sqrt[3]{q_T} = \sqrt[3]{2} \approx 1.25\,. \tag{3}$$

shows that the length growth factor and the axis height $q_h = 1.25$ which corresponds with the growth factor of the order R10 or R20/2.

Rational coverage of the whole range of the projected assortment is done if the universal reducer family is observed with this value of the growth factor (Fig. 2).

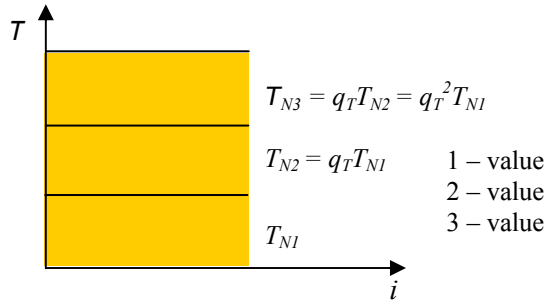

Fig. 2 . Graphical interpretation of areas which covers different values of the universal gear reducers

One can see from Fig. 2 the areas which cover different values of the universal gear reducers.

Call-out names for rotary moments (T_N) are not the same with respect to producers. However, producers are trying to generalize the values to make possible the interchange of the reducers. This is done by the same or similar connecting dimensions. In this way producers are trying to gain the market advantage.

1. Increase of the transmission ratio (*i*) of the reducers:

- leaving the concept of coaxial reducers,
- manufacturing driving sprocket with small number of teeth (z < 10),
- press of the first sprocket on the shaft or bushing which is placed on the electromotor shaft instead of placing it on the shaft,
- installing sprockets with big diameter into the reducers housing by opening the fast and/or slow chamber etc.

2. Increase of the reducers load – T_N:

- implementing higher quality materials,
- implementing higher quality of mechanical and thermo-chemical processes,
- increase of the modules,
- implementing two sets of sprockets in the same housing (smaller transmission ration with bigger and bigger transmission with a smaller load.

3. Increase of efficient coefficient (η):

- decrease of number of transmission couples,
- higher quality and bigger precision manufacturing,
- use of higher quality of (synthetic) oil, etc.

4. Decrease of the reducer noise and vibration

- increase of the contact coefficient by increase of the helix angle,
- more precise and quality fabrication.

5. Increase of reliability and the product life span:

- more accurate calculation (method of finite elements),
- more precise and quality fabrication,
- use of higher quality materials, etc.

6. Mass decrease

- more accurate calculations (method of finite elements),
- rational approach in component modeling,
- use of higher quality materials.

7. Cut of production costs

- using up to date conceptual solutions for reducers,
- using modern production technology,
- better work organization.

8. Increase of universality:

- using up to date conceptual solutions for reducers,
- lowering the number of different parts.

9. Increase of possibility for recycling:

- Implementing modern reducer solutions which will offer simple disassembly and material unification.

10. Ecological demands:

- implementing modern reducer solution which will lower the possibility for lubricant leakage,
- implementing good quality seals,
- implementing less toxic lubricants,
- implementing production technology which is less pollutant to human environment.

11. Design improvement:

- devoting more attention to part design,
- devoting more attention to reducer color,
- by using modern graphical means of information which are placed on the reducer, on its packaging and its documentation.

Of course, these demands are also fulfilled by the competition, and therefore, it is very hard maintaining a successful producer.

For these reasons, leading reducer manufacturers are leaning towards radical decisions by manufacturing midsize reducers, which demand bigger financial investments. Smaller manufactures can not afford this, thus in some market segments bigger manufactures can offer cheaper solutions and gain the buyers. Since most of the buyers want to obtain all reducers from the same supplier, even from the same producer, they acquire the rest of the reducers, which are with the same or similar price like the competition, from the same manufacturer which gives a direct gain to the producer who introduced the midsize reducer. Characteristics of these midsizes are shown in the Fig. 3.

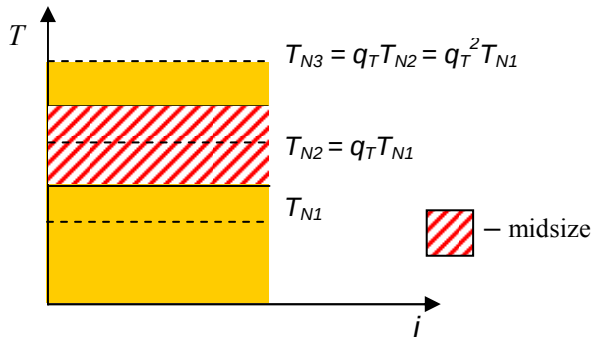

Fig. 3. Graphical interpretation of the area which covers one characteristic midsize of the universal gear reducer

By this approach, big producers gain some advantage in the area with most wanted sizes since they can offer a smaller (cheaper) reducer in 50% is not for underestimating. Of course, this disturbs the order which economically is justified because big producers have large lines and a midsize so they can treat it as a standard size in the same reducer family.

The load interval and the gear ration in which the midsize is decided are dictated by the market. Most wanted sizes are universal gears with the mid size, whereas small and big gears are relatively less wanted. Small gears are made as special gears when small gears are wanted in large series. Of course, producers of universal gears are interested in manufacturing special gears when large series are in question.

Most wanted gear ratios are the ones with a mid size which are covered by two ratio gears which have an ability for high gear ratio, or, if it is not possible, then three ratio gears with small gear ratios.

Which solution is picked, depends on the adopted reducer concept line. All large producers manufacture one, two, three, or multiratio gear reducers. Small producers, mainly, do not make one ratio reducers since it is a small market. Two and three ratio reducers are made with the same box, whereas, multiratio reducers are combined of two and three ratio gears. Multiratio reducers are not made from joining multiple reducer boxes, and they are made as separate reducers. Their demand is very low, thus most of the large producers do not offer them. Specialized producers make them.

There should be the same coverage of power for the two and three ratio reducers as for the rest members of the line.

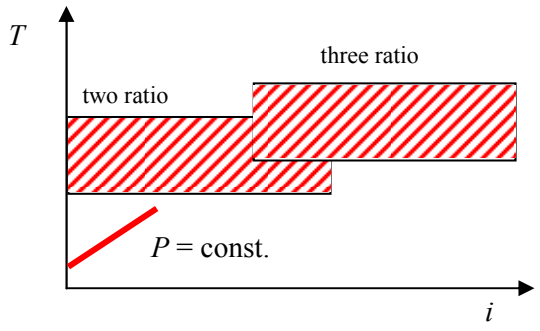

Fig. 4. Graphical interpretation of the area which covers one characteristic mid size for two and three universal gear reducers

With this approach one uses advantages of mid the size. Nowadays producers also make an electromotor, therefore they offer motor reducers, which offer all advantages.

Reducer producers also demand to make special reducer electro motors with different flanges diameter and electro motor shaft end. Thus, they can connect one reducer with different electromotor powers, or in case of usage of standards of IEC motors, then they have to supply with adapters for IEC motors which will solve the problem of connecting different sizes of motor and reducers. This additionally complicates the production but still is payable.

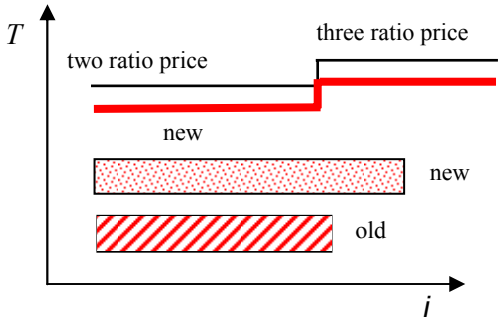

Fig. 5. Graphical interpretation of the area which covers one mid size characteristic of two ratio universal gear reducer and its prices

The increase of the biggest gear ratios influences the production costs. Bigger sprockets are always offered. There are already gears with gear ratios up to i = 12.5 (LENZE). Whith this approach, one ratio reducers in the area in which competition offers one ratio reducers are more expensive, while in the area where competition offers two ratio reducers are cheaper. Therefore, manufacturers of these reducers, to have a good business, offer them with the same price as the competition or lower, and in the area of two ratio reducers, offer them with higher prices but lower than the competition. The same goes for two (Fig. 5) or higher ratio reducers.

With these and similar approaches, leading reducer manufacturers strive to secure successful marketing of their reducers and to secure their future on the reducer market.

CONCLUSION

Based on this analysis, one can see that it is justified to introduce mid sizes since it is possible in most of the cases to have cheaper solution. This will attract buyers who would buy the size that is not the cheapest but it is from the same manufacturer, from which that manufacturer has an advantage.

The gool of analysis this is to encourage small manufacturers to start thinking of expanding their reducer assortment.

LITERATURE

[1] S. Kuzmanović, *Univerzalni zupčasti reduktori sa cilindričnim zupčanicima*, Fakultet tehničkih nauka, Novi Sad, 2002.

[2] S. Kuzmanović, *Menadžment proizvodima*, Ekonomski fakultet, Subotica 2004.

[3] Д. Стамболиев, *Основи на конструирањето*, Машински факултет, Скопје, 1987.

Р е з и м е

АНАЛИЗА НА ОПРАВДАНОСТА НА ДОПОЛНУВАЊЕТО НА АСОРТИМАНОТ НА УНИВЕРЗАЛНИТЕ ЗАПЧЕСТИ РЕДУКТОРИ

Синиша Кузмановиќ[1], Петар Симоновски[2]

[1]Факултет за технички науки, Трг Доситеја Обрадовиќа 6, Нови Сад, Република Србија
[2]Машински факултет, Универзитет „Св. Кирил и Методиј“,
п. фах 464, МК-1001 Скопје, Република Македонија
kuzman@uns.ns.ac.yu // pero@mf.edu.mk

Клучни зборови: анализа; асортиман; универзален; запчест редуктор

Во трудот е анализирана проблематиката на дополнувањето на асортиманот на универзалните запчести редуктори со проширување на постојните редови. Имено, познато е дека на пазарот со универзални запчести редуктори е присутна силна конкуренција и повеќето производители тежнеат својот асортиман на производи да го зголемат за што повеќе да ги задоволат побарувањата на пазарот. Во рамките на овој труд се посочуваат на некои од можностите за разрешување на тој проблем.

Mechanical Engineering – Scientific Journal, Vol. **28**, No. 1, pp. 35–38 (2009)
CODEN: MINSC5 – 406 ISSN 1857–5293
Received: April 15, 2009 UDK: 621.313 : 004.822
Accepted: April 21, 2009

Original scientific paper

NEURAL NETWORK EXPLOITATION IN RELIABILITY ASSURANCE

Ján Kadák, Imrich Andrejčák, Júlia Mečiarová

Faculty of Environmental and Manufacturing Technology, Technical University in Zvolen, Studentska 26, SK-960 53 Zvolen, Slovakia
andrejcak@vsld.tuzvo.sk

A b s t r a c t: The contribution deals with neural network application for the diagnostic system of the three-phase asynchronous electromotor. The case study is done and can be used as a model for the next application of neural network methodology.

Key words: neural network; three-phase asynchronous electromotor; reliability

1. INTRODUCTION

Over the past years, several technologies have been introduced to help engineers to analyze and design complex systems. One of these techniques is artificial neural network technology. The artificial neural network (ANN) is a young discipline of science, but it is necessary to respect the intensity of its development.

The purpose of the ANN application is the imitation of a human thinking by solution of a specific problem. Another advantage for the ANN application is the ability of its adaptation to the situation and environment changes. The possibility of incomplete data processing is anomalous.

The ANN technology has become very popular and is used in many fields. In the field of reliability assurance of machines and facilities it can be applied in technical diagnostics, which deals with the application of diagnostic equipments during the normal function of objects (facilities).

The task of the proposed diagnostic system is to detect the risk of possible failure and to stop working the controlled object on time. For this purpose, physical diagnostic methods are used. The changes of observed properties are being evaluated to predict the possible risk of critical situation occurrence. For example, by the bearing lubrication controlling: if some observed parameter (oil pressure, bearing temperature) changes out of limits, the critical state is signaling and it comes to corrections.

Some applications are possible by the implementation of hardware neural networks (neuro-processors) in the computer control of automatic diagnostic stations. The whole diagnostic system is then controlled by a computer, which is directly connected with controlling object operations. It informs about actual operation state, maintenance and it provides systematic data capturing about reliability of functional parts of the object.

2. NEURAL NETWORK DESIGN

For the practical example of a possible neural network design, a three-phase asynchronous electromotor has been chosen, because it is included in many machines and facilities. The motor works by the temperature of 21 degrees. The proposed neural network will serve as an evaluation system, which on the basis of measured parameters detects possible failure and prevent damage. To simplify the problem, the task does not deal with the measuring of parameters. The input parameters for the ANN are customized signals from sensors. The output from ANN is numeric information about the actual state of observed parts of the electromotor. To each defined number correspondents some text information.

Technical data of the electromotor

Type: Siemens 1LA7 130-4AA10, IM B3, supply voltage: ~3×400 V / 50 Hz, power: 5.5 kW, engine speed: n = 1455 min^{-1}, synchronous speed: n_s = 1500 min^{-1}, number of couple pole: p = 4, environment temperature: –30°C to +40°C, weight 42.5 kg [6].

Measured parameters are:

– Overall vibration of the motor – is expressed by the effective value of the vibration speed v_{ef} (mm.s^{-1}), which is measured in horizontal direction vertically to the shaft. Allowed value for the electromotor is 2.8 mm.s^{-1}.

– Amplitude spectral density $|F(f)|$ (dB). By the spectral analysed used, the incipient failure of some parts (e.g. unbalance, failure of bearings) has been localized. In this case, the broken or released rotor shafts are observed, because they can generate vibrations. This effect becomes evident in the spectrum by increasing secondary zones in the network frequency environment (50 Hz). The value of these secondary zones is ±3 Hz by using this electromotor. If the difference of the amplitude spectral density by frequencies of 50 and 53 Hz (47 Hz) decreases under 45 dB, the system indicates a serious error.

– Temperature of front bearing T_{lf} (°C) and back bearing (near ventilator) T_{lr} (°C). The temperature is being measured and by the increased value the system informs about possible failure. The allowed value for this type of bearings (type 6208 2Z C3) is 120 degrees.

The training data for the neural network are shown in Table 1.

Data from the table were proccessed by software STATISTICA Automatizované neurónové síte CZ (5). With special tools using, several neural networks – type MLP (Multilayer Perceptrons) were created.

Table 1

Input and output data for ANN

Example	v_{ef} mm.s^{-1}	$\|F(50)\| - \|F(53)\|$ dB	T_{lf} °C	T_{lr} °C	State	State definition
1	1,1	60	40	30	1	Faultless
2	1,3	55	49	32	2	Good
3	1,5	60	68	58	3	Bad
4	2,9	43	45	35	4	Critical
5	3	40	47	36	4	Critical
6	3,5	52	138	38	4	Critical
7	3,2	53	46	125	4	Critical
8	4,1	48	129	123	4	Critical
9	5,1	41	130	127	4	Critical
10	2,8	50	42	43	3	Bad

From these networks, one ANN has been chosen, which best fitted the criteria of the minimum training error. This ANN consists of four input neurons, nine hidden neurons and one output neuron. Some connections and weight values between neurons are shown in the Table 2.

Table 2

Individual connections and weights between neurons

v_{ef} (mm·s^{-1}) —> hidden neuron 1	–0.03467	|F(50)| – |F(53)| (dB) —> hidden neuron 1	–0.06109
v_{ef} (mm·s^{-1}) —> hidden neuron 2	0.05063	|F(50)| – |F(53)| (dB) —> hidden neuron 2	0.07259
v_{ef} (mm·s^{-1}) —> hidden neuron 3	–0.04282	|F(50)| – |F(53)| (dB) —> hidden neuron 3	0.13751
v_{ef} (mm·s^{-1}) —> hidden neuron 4	0.00448	|F(50)| – |F(53)| (dB) —> hidden neuron 4	0.01005
v_{ef} (mm·s^{-1}) —> hidden neuron 5	–0.00583	|F(50)| – |F(53)| (dB) —> hidden neuron 5	–0.08540
v_{ef} (mm·s^{-1}) —> hidden neuron 6	–0.01966	|F(50)| – |F(53)| (dB) —> hidden neuron 6	–0.03194
v_{ef} (mm·s^{-1}) —> hidden neuron 7	–0.03473	|F(50)| – |F(53)| (dB) —> hidden neuron 7	–0.00814
v_{ef} (mm·s^{-1}) —> hidden neuron 8	–0.02064	|F(50)| – |F(53)| (dB) —> hidden neuron 8	0.30810
v_{ef} (mm·s–1) —> hidden neuron 9	0.10031	|F(50)| – |F(53)| (dB) —> hidden neuron 9	–0.20215
T_{lf} (°C) —> hidden neuron 1	0.10039	T_{lr} (°C) —> hidden neuron 1	–0.01532
T_{lf} (°C) —> hidden neuron 2	–0.10242	T_{lr} (°C) —> hidden neuron 2	–0.01099
T_{lf} (°C) —> hidden neuron 3	–0.18504	T_{lr} (°C) —> hidden neuron 3	–0.01525
T_{lf} (°C) —> hidden neuron 4	0.11850	T_{lr} (°C) —> hidden neuron 4	–0.01055
T_{lf} (°C) —> hidden neuron 5	–0.09211	T_{lr} (°C) —> hidden neuron 5	–0.01755
T_{lf} (°C) —> hidden neuron 6	0.06817	T_{lr} (°C) —> hidden neuron 6	–0.02593
T_{lf} (°C) —> hidden neuron 7	–0.01128	T_{lr} (°C) —> hidden neuron 7	0.05410
T_{lf} (°C) —> hidden neuron 8	0.01548	T_{lr} (°C) —> hidden neuron 8	0.01347
T_{lf} (°C) —> hidden neuron 9	–0.03780	T_{lr} (°C) —> hidden neuron 9	–0.02231
input part —> hidden neuron 1	6.85293	hidden neuron 1 —> state	–0.22940
input part —> hidden neuron 2	–1.02415	hidden neuron 2 —> state	0.09207
input part —> hidden neuron 3	3.30132	hidden neuron 3 —> state	0.15536
input part —> hidden neuron 4	–0.10755	hidden neuron 4 —> state	0.27131
input part —> hidden neuron 5	6.63726	hidden neuron 5 —> state	0.08191
input part —> hidden neuron 6	5.40444	hidden neuron 6 —> state	0.69203
input part —> hidden neuron 7	–0.54379	hidden neuron 7 —> state	0.00472
input part —> hidden neuron 8	–0.47704	hidden neuron 8 —> state	0.02446
input part —> hidden neuron 9	–0.09159	hidden neuron 9 —> state	–0.26268
		hidden part —> state	0.12864

Graphics environment of ANN in program STATISTICA Automatizované neurónové síte CZ is depicted in Fig. 1..

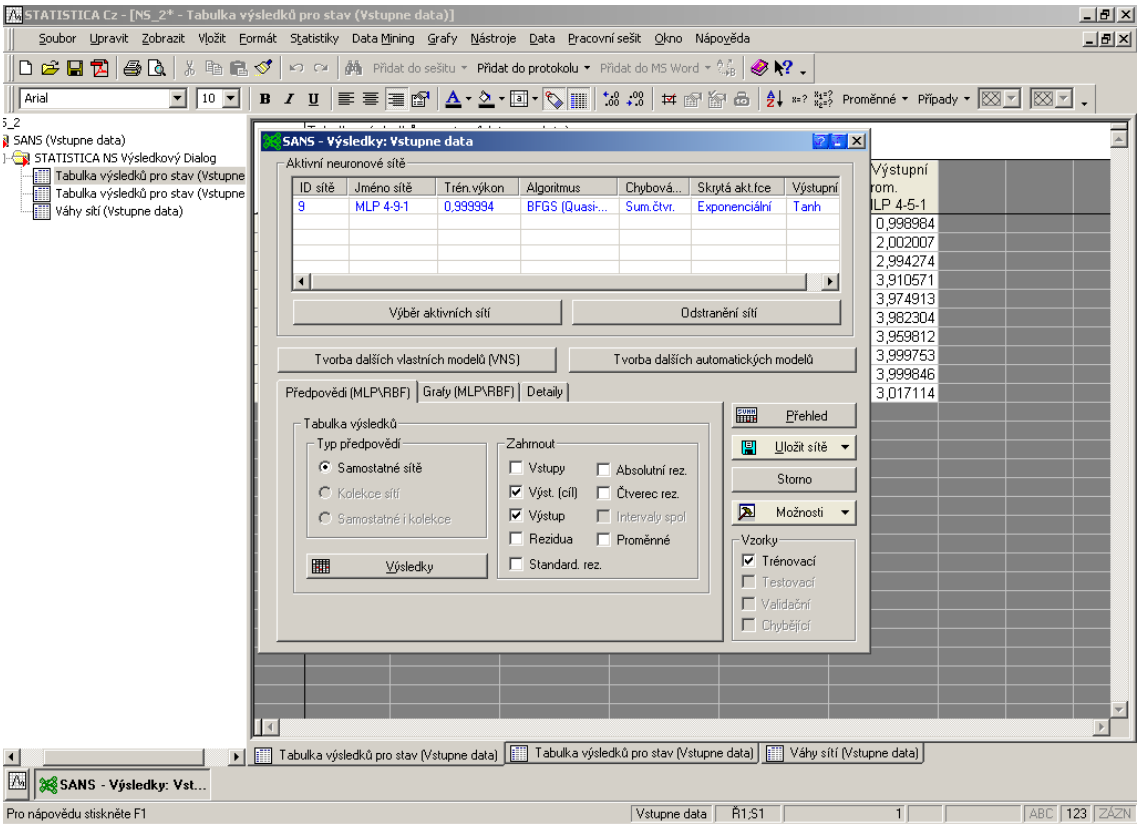

Fig. 1. Proposed neural network in program STATISTICA (5)

3. DISCUSSION

This all shows that the accuracy of network results depends on the amount of training models. This case study expresses the way, how the neural networks can be designed and simulated. This proposed model does not include the testing of training models, but only training of given models of inputs and outputs. By the training set of input-output data we can determine the output value variation from desired value. In the case of different output parameters, we can modify the weights that the difference between actual and desired value is minimal. The advantage of STATISTICA Automatizované neurónové síte CZ is the support of automated creation, training and testing of neural networks.

4. CONCLUSION

In this contribution, a neural network application in operating diagnostics of a three-phase asynchronous electromotor is proposed. The case study is very simple and can be used as a model for the next development of neural network study.

This article was created under the Grant No. 1/0511/08 supported by the Ministry of Education of Slovak Republic.

REFERENCES

[1] Marcel Kreidl, Radislav Šmíd, *Technická diagnostika.* Praha: BEN technická literatura, 2006. 408 p. ISBN 80-7300-158-6

[2] Vladimír Kvasnička, et al.: *Úvod do teórie neurónových sietí.* Bratislava: IRIS, 1997. 285 p. ISBN 80-88778-30-1

[3] Ľudovít Šipoš, Tibor Csongrády, *Umelá inteligencia.* Zvolen: TU Zvolen, 2006. 99 p. ISBN 80-228-1591–8

[4] Peter Sinčák, Gabriela Andrejková, *Neurónové siete. Inžiniersky prístup I.* (online]. Košice: TU Košice, 1996. (cit. 2008-02-22]. <http://www 2.fiit.stuba.sk/~cernans/nn/nn_download/Sincak_Andrejkova_vol_1.pdf>

[5] Firma StatSoft s.r.o. CR: *STATISTICA Automatizované neurónové síte.* (online]. (cit. 2007-12-24]. <http://statsoft.cz/page/index2.php?pg=navigace&id=47>

[6] D. Kalincová, O. Barborák, I. Andrejčák, Využitie technológií neurónových sietí, *9. Medzinárodná vedecká konferencia, Trenčín,* 18–19. September 2007, Transfer

[7] Firma Siemens, Slovensko: *Katalóg trojfázových asynchrónnych motorov.* (online]. (cit. 2007-12-29]. <http:// www.siemens.com/Daten/siecom/ Slovakia/WebTeam/Intranet/Business/A_D/WORKAREA/sk2a_d/templatedata/ Slovak/file/binary/k02-0404-katalog-1la7-cz_2000001344543.pdf>

Р е з и м е

КОРИСТЕЊЕ НА НЕВРОНСКИ МРЕЖИ ЗА ОБЕЗБЕДУВАЊЕ НА ДОВЕРЛИВОСТ

Јан Кадак, Имрих Андрејчак, Јулиа Мечиарова

Faculty of Environmental and Manufacturing Technology, Technical University in Zvolen, Studentska 26, SK-960 53 Zvolen, Slovakia
andrejcak@vsld.tuzvo.sk

Клучни зборови: невронски мрежи; електромотор; доверливост

Во трудов е презентирана примена на невронска мрежа за дијагностички систем на трифазен асинхрон електромотор. Прелиминарното истражување е завршено и може да биде користено како модел на методологијата за користење на невронски мрежи.